RESEARCH ARTICLE • OPEN ACCESS

Stem Cell Based Fractional-Order Dynamical Model of Psoriasis: A Mathematical Study

Subhankar Kushary *et al.*

Volume 6, Issue 3, Pages 200–221, September 2025

Received 1 July 2025, Revised 1 August 2025, Accepted 2 August 2025, Published Online 1 September 2025

To Cite this Article : S. Kushary *et al.*,"Stem Cell Based Fractional-Order Dynamical Model of Psoriasis: A Mathematical Study", *Jambura J. Biomath*, vol. 6, no. 3, pp. 200–221, 2025, *https://doi.org/10.37905/jjbm.v6i3.33134*

JOURNAL INFO • JAMBURA JOURNAL OF BIOMATHEMATICS

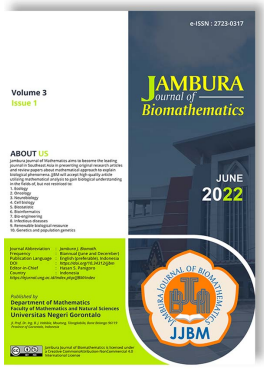

Homepage	:	http://ejurnal.ung.ac.id/index.php/JJBM/index
Journal Abbreviation	:	Jambura J. Biomath.
Frequency	:	Quarterly (March, June, September and December)
Publication Language	:	English
DOI	:	https://doi.org/10.37905/jjbm
Online ISSN	:	2723-0317
Editor-in-Chief	:	Hasan S. Panigoro
Publisher	:	Department of Mathematics, Universitas Negeri Gorontalo
Country	:	Indonesia
OAI Address	:	http://ejurnal.ung.ac.id/index.php/jjbm/oai
Google Scholar ID	:	XzYgeKQAAAAJ
Email	:	editorial.jjbm@ung.ac.id

JAMBURA JOURNAL • FIND OUR OTHER JOURNALS

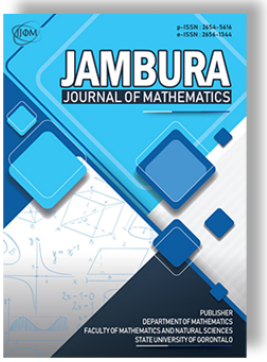

Jambura Journal of Mathematics

Jambura Journal of Mathematics Education

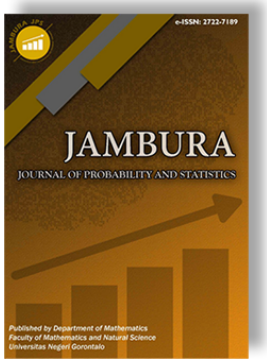

Jambura Journal of Probability and Statistics

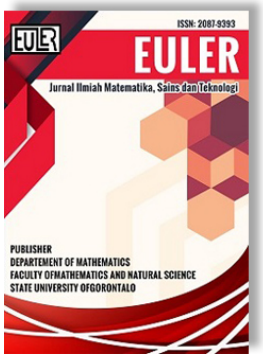

EULER : Jurnal Ilmiah Matematika, Sains, dan Teknologi

Jambura Journal of Biomathematics, Volume 6, Issue 3, Pages 200–221, September 2025 https://doi.org/10.37905/jjbm.v6i3.33134

Research Article

Check for updates

Stem Cell Based Fractional-Order Dynamical Model of Psoriasis: A Mathematical Study

Subhankar Kushary[1], Tushar Ghosh[1], Oluwole Daniel Makinde[2], Xue-Zhi Li[3], and Priti Kumar Roy[1,*]

[1]*Center for Mathematical Biology and Ecology, Dept. of Mathematics, Jadavpur University, Kolkata, West Bengal, India*
[2]*Faculty of Military Science, Stellenbosch University, Private Bag X2, Saldanha, 7395, South Africa*
[3]*College of Statistics and Mathematics, Henan Finance University, Xinyang, 464000, China.*

ARTICLE HISTORY
Received 1 July 2025
Revised 1 August 2025
Accepted 2 August 2025
Published 1 September 2025

KEYWORDS
Psoriasis
Fractional order differential equations
Optimal control
Forward-Backward sweep method

ABSTRACT. *Psoriasis is a chronic autoimmune skin disorder driven by dysregulated immune responses, where abnormal interactions between T cells and dendritic cells lead to excessive inflammatory cytokine production. This triggers the hyper-proliferation of epidermal keratinocytes while depleting mesenchymal stem cells (MSCs), which play a crucial role in immune modulation. The progression behavior of psoriasis is not only influenced by their present state but also by the historical evolution of underlying cellular interactions. Memory stages and complex interplay among immune components at different temporal scales significantly modulate disease expression. Motivated by this, we proposed a mathematical model of psoriasis to a fractional-order framework in order to incorporate memory-dependent effects and non-local characteristics. This article deals with a four-dimensional model of psoriasis involving concentrations of T cells, dendritic cells, keratinocytes, and mesenchymal stem cells (MSCs) in order to predict the temporal evolution in the considered cell densities during the disease dissemination process. Using Caputo, Caputo-Fabrizio, and Atangana-Baleanu-Caputo operators, we analyze how memory influences disease dynamics. In-depth mathematical analysis of the solution of the fractionalized model has been thoroughly investigated. The stability of the model is also examined using generalized Ulam–Hyers stability criteria. The considered population densities are numerically evaluated using various fractional orders with considered fractional operators to capture non-local effects. Optimal control is implemented on the fractionalized system using the Forward-Backward Sweep Method (FBSM), emphasizing the impacts of two biologics, namely TNF-α inhibitors and IL-23 blockers, via considered operators. Numerical simulations are performed in support of the theoretical analyses, accompanied by detailed discussions from both mathematical and biological viewpoints. Results based on optimal control effectiveness analysis indicate that a combined control strategy, particularly under the Caputo-Fabrizio operator, optimally reduces keratinocyte density. Which offers deeper insights into disease progression and effective therapeutic approaches.*

1. Introduction

Psoriasis is a chronic dermatological disorder characterized by excessive growth of epidermal cells resulting in scaly silvery or red patches on the skin. Several factors are associated with this growth. Mainly, the immune system plays a central role in mediating autoimmune responses that lead to the progression of the disease. Although it is not fatal, severe forms of the disease can lead to significant social stigma and ostracism [1]. This condition profoundly impacts patients' quality of life, often contributing to socioeconomic challenges, mental health disturbances, and an increased risk of depression. Psoriasis affects less than 1 % of the global pediatric population, while its prevalence among adults varies geographically, ranging from 0.17 % in East Asia to 2.5 % in Western Europe [2]. Risk factors such as consumption of alcohol, smoking habits, and obesity are associated with severe manifestations of the disease in affected individuals. The complex interplay between T cells, dendritic cells (DCs), and the cytokines they secrete plays a pivotal role in the pathogenesis of psoriasis. Epidermal hyper-proliferation, abnormal differentiation of immune cells and keratinocytes, and inflammatory cell infiltration are the key features of this skin disease [3].

T cells are the kind of white blood cells that are an important component of the human immune system. In psoriasis, dysfunctional DCs (antigen-presenting cells) activate T cells through cytokines such as Tumor necrosis factor-α (TNF-α), Interleukin-12 (IL-12), and Interleukin-23 (IL-23), which promote the differentiation of T cell subsets, primarily Th_1 and Th_{17} [4]. Furthermore, malfunction of T cells stimulates DCs via abnormal release of TNF-α and IL-17. Under normal homeostasis, keratinocytes (the predominant keratin-presenting cells in the epidermis) protect the body from external threats and help in wound healing processes. However, in psoriasis, keratinocytes become passive targets that are triggered by the mutual interaction of T cells and DCs via cytokines. These inflammatory cells and cytokine storms eventually infiltrates, which promotes the hyper-proliferation and con-

*Corresponding Author.

Email : *pritiju@gmail.com* (P. K. Roy)
Homepage : http://ejurnal.ung.ac.id/index.php/JJBM/index / E-ISSN : 2723-0317

tributes to the growth of the keratinocyte population. In addition, interferon-γ (IFN-γ), a pivotal cytokine whose secretion is induced by IL-12, promotes DC maturation and the activation of TNF-α through specific cellular pathways [5]. Recent studies have demonstrated that IL-23 directly induces the production of IL-22, which regulates keratinocyte differentiation and migration [6]. The cytokines TNF-α and IFN-γ, in conjunction with the IL-17/22 axis, create a synergistic feedback loop that enhances keratinocyte growth factors, which leads to the development of psoriatic inflammation [7]. Stem cells, a unique type of cell and are essential for tissue development and repair after injury [8]. Embryonic stem cells and adult stem cells are the two primary subtypes of stem cells. Mesenchymal stromal cells (MSCs) are one kind of adult stem cell present in diverse tissues, including the umbilical cord, bone marrow, and adipose tissues. MSCs have anti-inflammatory properties and can modulate cytokine secretion in various autoimmune conditions. They prevent the infiltration of inflammatory cells into affected regions by secreting immunoregulatory cytokines such as Transforming growth factor-β (TGF-β) and IL-10 and reduce the expression of pro-inflammatory cytokines like TNF-α, IL-12, and IL-23 [9].

To deal with psoriasis effectively, it is very important to identify the key factors that trigger and influence disease progression. Evaluating the efficacy of various treatment strategies to help patients cope with this condition is equally important. Mathematical models offer valuable tools for predicting disease severity, future manifestations, and the impact of different therapeutic interventions. Recently, several researchers have focused on psoriasis through the development of mathematical models, aiming to better understand its dynamics and optimize treatment approaches. Sherratt et al. [10] introduced a mathematical model incorporating nitric oxide (NO) concentrations and extended it by considering NO regulates the formation of rete pegs in psoriatic plaques. Oza et al. [11] used the framework to model cytokines as fast finite-time actuators, employing perturbation theory to demonstrate the dynamics of their model, which are finite-time convergent to a particular equilibrium point instead of asymptotically convergent. Zhang et al. [12] developed a computational model addressing keratinocyte proliferation, differentiation, and apoptosis to investigate the spatio-temporal dynamics of epidermal homeostasis. Roy and his group investigated the role of cytokine signaling within cellular networks to construct mathematical models of psoriasis, applying optimal control strategies to examine the impact of key cytokines [13]. Recently, they have proposed the application of stem cell therapy as a potential future treatment option for remission of psoriasis [14].

Since 2007, several biologic therapies have been approved for the treatment of psoriasis. Among these, two classes of biologics are widely used for controlling moderate to severe cases: TNF-α inhibitors (e.g., Adalimumab, Etanercept, Infliximab) and IL-23 inhibitors (e.g., Ustekinumab, Guselkumab). These cytokine-targeting agents have demonstrated effective therapeutic outcomes; however, their efficacy varies between individuals [15]. In clinical practice, combination therapies are often employed based on patient-specific needs [16]. From a modeling perspective, these treatments are implementable control measures, as they represent feasible and clinically proven therapeutic options.

Earlier mathematical models of psoriasis predominantly employed integer-order differential equations, recent studies highlight the superiority of fractional-order models [17, 18]. Fractional-order systems, owing to their non-local nature and ability to incorporate memory effects, provide a more accurate and comprehensive framework for modeling immune system interactions. Agarwal et al. [19, 20] presents a fractional-order bone mineralization model using Caputo derivatives, analyzed qualitatively and highlighting the model's memory effect and its potential to better fit experimental data and provide insights into disease-related deviations in bone mineral patterns. Musafir et al. [21] present a comparison fractional-order monkeypox model with singular and non-singular kernels. Kalyan das et al. [22] present a qualitative analysis of the leukemia fractional order SICW model. They establish key mathematical properties, validate through real data, and demonstrate through simulations and optimal control that fractional-order dynamics enhance forecasting accuracy and intervention effectiveness. Ghosh et al. [20] develop a fractional-order childhood disease model using Caputo operators and analyze the dynamic impact of fractional calculus on infectious disease modeling. Recently they employed the Homotopy Perturbation Transform Method (HPTM) in the hepatitis B model [23]. They have used the Katugampola fractional operator in the Caputo sense to efficiently obtain solutions of a mathematical model and analyze a fractional-order model. Motivated by these, we undertook the present study.

2. Overview of the Work

In this study, we extend our previously proposed psoriasis model [24] by formulating and analyzing its fractional-order counterparts using three distinct operators: Caputo, Caputo–Fabrizio, and Atangana–Baleanu in the Caputo sense. These formulations incorporate memory effects, which are critical in capturing autoimmune responses and cytokine-driven disease progression. The fundamental mathematical properties are also described for the fractionalized model, and the influence of memory is assessed through a comparative analysis of the considered operators. Further, we investigate the optimal control problem involving two biologic inhibitors and evaluate the effectiveness of three different control strategies through numerical simulations. These simulations highlight the distinct non-local dynamics introduced by each operator. However, due to limited clinical data at the cellular level, we were unable to validate the model or perform error analysis among the three operators, which we acknowledge as a limitation of this work.

3. Preliminaries of Fractional Calculus

Definition 1. [25] Let $f(t)$ be a function that is n-times continuously differentiable on the interval $[0, T]$, where $n = \lceil \lambda \rceil$ is the smallest integer greater than or equal to the fractional order $\lambda > 0$. The Caputo fractional derivative of order λ, denoted by ${}^{C}D_t^{\lambda} f(t)$, is defined as:

$$ {}^{C}\mathcal{D}_t^{\lambda}[f(t)] = \begin{cases} \dfrac{1}{\Gamma(n-\lambda)} \displaystyle\int_0^t \frac{f^{(n)}(s)}{(t-s)^{\lambda-n+1}}\, ds, & n-1 < \lambda < n, \\ \dfrac{d^n f(t)}{dt^n}, & \lambda = n \in \mathbb{N}, \end{cases} $$

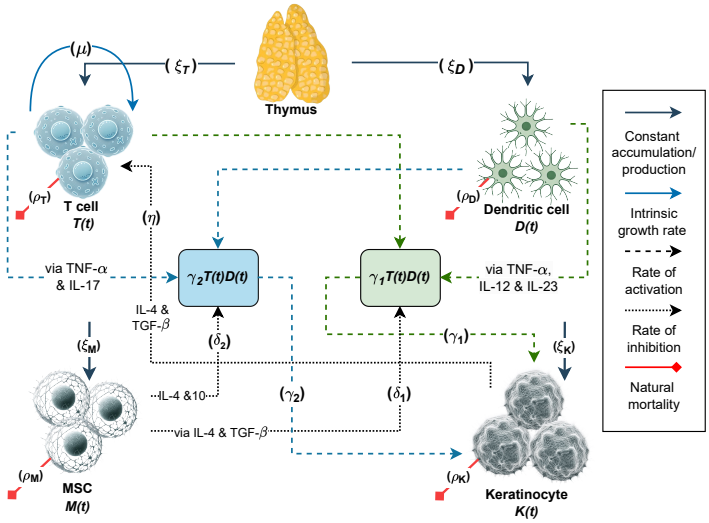

Figure 1. Schematic representation of the model within a cytokine network.

where $\Gamma(\cdot)$ denotes the Gamma function.

Definition 2. [26] Let $f(t) \in C^1([0,T])$ be a continuously differentiable function on the interval $[0,T]$, and let $\zeta \in (0,1)$ be the fractional order. The Caputo–Fabrizio fractional derivative of order ζ, is defined as follows:

$$^{CF}\mathcal{D}_t^{\zeta}[f(t)] = \frac{N(\zeta)}{1-\zeta}\int_0^t f'(s)\exp\left[-\zeta\frac{t-s}{1-\zeta}\right]ds, t>0,$$

where $N(\zeta)$ is a normalization constant such that $N(0) = N(1) = 1$.

Definition 3. [27] Consider a real-valued function $f : [0,T] \to \mathbb{R}$ such that $f \in \mathcal{H}^1(0,t)$, where $\mathcal{H}^1(0,t)$ denotes the Sobolev space of functions with square-integrable first derivatives:

$$\mathcal{H}^1(0,t) = \left\{f \in L^2(0,t) \mid f' \in L^2(0,t)\right\}.$$

The Atangana-Baleanu fractional derivative in the Caputo sense of order $\alpha \in [0,1)$ is defined by

$$^{ABC}\mathcal{D}_t^{\alpha}[f(t)] = \frac{\mathbf{B}(\alpha)}{1-\alpha}\int_0^t f'(s)\mathbf{E}_{\alpha}\left[-\frac{\alpha}{1-\alpha}(t-s)^{\alpha}\right]ds,$$

where $\mathbf{E}_{\alpha}(\cdot)$ is the one-parameter Mittag-Leffler function and the normalizing function $\mathbf{B}(\alpha)$ is given by

$$\mathbf{B}(\alpha) = 1-\alpha+\frac{\alpha}{\Gamma(\alpha)}.$$

Definition 4. [27] Let $f \in \mathcal{H}^1(0,t)$, and $\alpha \in [0,1]$. The Atangana-Baleanu-Caputo fractional integral operator of order α is defined as

$$^{ABC}I_t^{\alpha}[f(t)] = \frac{1-\alpha}{\mathbf{B}(\alpha)}f(t)+\frac{\alpha}{\mathbf{B}(\alpha)\Gamma(\alpha)}\int_0^t f(s)(t-s)^{\alpha-1}ds.$$

Lemma 1. *[27] Let $\alpha \in [0,1]$. If the Atangana-Baleanu-Caputo derivative satisfies*

$$^{ABC}\mathcal{D}_0^{\alpha}\mathcal{H}(t) = \mathcal{J}(t,\mathcal{H}(t)), \quad t\in(0,T), \quad \mathcal{H}(0)=\mathcal{H}_0,$$

then the function $\mathcal{H}(t)$ is given by

$$\mathcal{H}(t) = \mathcal{H}_0+\frac{1-\alpha}{\mathbf{B}(\alpha)}f(t)+\frac{\alpha}{\Gamma(\alpha)\mathbf{B}(\alpha)}\int_0^t f(s)(t-s)^{\alpha-1}ds.$$

Lemma 2. *[28] Assume that $z : [0,t_f] \to \mathbb{R}$ and $0 < \alpha \leq 1$. Then, the following identity holds:*

$$^{F}_{t}D^{\alpha}_{t_f}z(t) = {}^{F}_{0}D^{\alpha}_{t}z(t_f-t),$$

where $^{F}D^{\alpha}$ denotes the fractional derivative in Caputo sense.

Theorem 1 (Fixed Point Theorem for Existence). *[29] Let $\mathbb{X}$ be a convex subset of a Banach space $\mathcal{Z}$ and suppose operators $\mathcal{X}_1, \mathcal{X}_2 : \mathbb{X} \to \mathbb{X}$ satisfy:*

1. *$\mathcal{X}_1 h + \mathcal{X}_2 h \in \mathbb{X}$ for all $h \in \mathbb{X}$,*
2. *$\mathcal{X}_1$ is a contraction,*
3. *$\mathcal{X}_2$ is compact and continuous.*

Then the operator equation $\mathcal{X}_1 h + \mathcal{X}_2 h = h$ has at least one solution in $\mathbb{X}$.

4. Fractional-Order Modelling Approach

Recent studies have increasingly highlighted the advantages of fractional-order systems across various disciplines, including finance, biochemical processes, epidemiology, fluid dynamics, and chemical and mechanical engineering. Fractional-order derivatives, owing to their ability to capture memory effects, often yield more accurate and realistic results than traditional integer-order models [30].

Based on the recent work proposed by Kushary et al. [24], we extend the classical integer-order model of psoriasis by incorporating three widely used fractional-order operators: the Caputo, Caputo–Fabrizio, and Atangana–Baleanu derivatives in the Caputo sense. In our model, $T(t)$, $D(t)$, $K(t)$, and $M(t)$ denote the concentrations of T cells, dendritic cells, keratinocytes, and mesenchymal stem cells (MSCs), respectively, at time t. The interactions among immune cells, keratinocytes, and MSCs, mediated by cytokines and contributing to disease progression, are illustrated in Figure 1. Accordingly, the proposed models corresponding to the aforementioned operators are formulated as follows:

4.1. The model with Caputo sense

$$\begin{aligned}
\mathcal{L}^{1-\lambda}\,{}^{C}D_t^{\lambda}[T(t)] &= \xi_T + \mu T(t)\left[1-\frac{T(t)}{T^{\max}}\right] - \frac{\gamma_1 T(t)D(t)}{1+\delta_1 M(t)} \\
&\quad - \eta T(t)K(t) - \rho_T T(t), \\
\mathcal{L}^{1-\lambda}\,{}^{C}D_t^{\lambda}[D(t)] &= \xi_D - \frac{\gamma_2 T(t)D(t)}{1+\delta_2 M(t)} - \rho_D D(t), \\
\mathcal{L}^{1-\lambda}\,{}^{C}D_t^{\lambda}[K(t)] &= \xi_K + \frac{\gamma_1 T(t)D(t)}{1+\delta_1 M(t)} + \frac{\gamma_2 T(t)D(t)}{1+\delta_2 M(t)} \\
&\quad \rho_K K(t), \\
\mathcal{L}^{1-\lambda}\,{}^{C}D_t^{\lambda}[M(t)] &= \xi_M - \rho_M M(t).
\end{aligned} \tag{1}$$

where $\lambda \in (0,1]$ is the fractional order for all the model population taken in the Caputo sense and 't' is time in days.

4.2. The model with Caputo-Fabrizio sense

$$\begin{aligned}
\mathcal{L}^{1-\zeta}\,{}^{CF}D_t^{\zeta}[T(t)] &= \xi_T + \mu T(t)\left[1-\frac{T(t)}{T^{\max}}\right] - \frac{\gamma_1 T(t)D(t)}{1+\delta_1 M(t)} \\
&\quad - \eta T(t)K(t) - \rho_T T(t), \\
\mathcal{L}^{1-\zeta}\,{}^{CF}D_t^{\zeta}[D(t)] &= \xi_D - \frac{\gamma_2 T(t)D(t)}{1+\delta_2 M(t)} - \rho_D D(t), \\
\mathcal{L}^{1-\zeta}\,{}^{CF}D_t^{\zeta}[K(t)] &= \xi_K + \frac{\gamma_1 T(t)D(t)}{1+\delta_1 M(t)} + \frac{\gamma_2 T(t)D(t)}{1+\delta_2 M(t)} \\
&\quad - \rho_K K(t), \\
\mathcal{L}^{1-\zeta}\,{}^{CF}D_t^{\zeta}[M(t)] &= \xi_M - \rho_M M(t).
\end{aligned} \tag{2}$$

where $\zeta \in (0,1]$ is the fractional order for all the model population taken in the Caputo-Fabrizio sense and 't' is time in days.

4.3. The model with Atangana-Baleanu-Caputo sense

$$\begin{aligned}
\mathcal{L}^{1-\alpha}\,{}^{ABC}D_t^{\alpha}[T(t)] &= \xi_T + \mu T(t)\left[1-\frac{T(t)}{T^{\max}}\right] - \frac{\gamma_1 T(t)D(t)}{1+\delta_1 M(t)} \\
&\quad - \eta T(t)K(t) - \rho_T T(t), \\
\mathcal{L}^{1-\alpha}\,{}^{ABC}D_t^{\alpha}[D(t)] &= \xi_D - \frac{\gamma_2 T(t)D(t)}{1+\delta_2 M(t)} - \rho_D D(t), \\
\mathcal{L}^{1-\alpha}\,{}^{ABC}D_t^{\alpha}[K(t)] &= \xi_K + \frac{\gamma_1 T(t)D(t)}{1+\delta_1 M(t)} + \frac{\gamma_2 T(t)D(t)}{1+\delta_2 M(t)} \\
&\quad - \rho_K K(t), \\
\mathcal{L}^{1-\alpha}\,{}^{ABC}D_t^{\alpha}[M(t)] &= \xi_M - \rho_M M(t),
\end{aligned} \tag{3}$$

where $\alpha \in (0,1]$ is the fractional order for all the model population taken in the Atangana-Baleanu-Caputo sense and 't' is time in days.

The initial conditions are given by

$$T(0) = T_0 > 0,\ D(0) = D_0 > 0,\ K(0) = K_0 > 0,\ M(0) = M_0 > 0.$$

In the fractional-order models (1) to (3), the terms ξ_T, ξ_D, ξ_K, and ξ_M represent the constant accumulation rates of T cells, dendritic cells, keratinocytes, and mesenchymal stem cells (MSCs), respectively. Since T cells cannot increase endlessly, the logistical expression $\mu T(t)(1-\frac{T(t)}{T^{\max}})$ highlights the growth of T cells, where μ is the proliferation rate and $T^{\max}$ is the maximum carrying capacity. The interaction term $\frac{\gamma_1 T(t)D(t)}{1+\delta_1 M(t)}$ represents a saturated incidence function, where $\gamma_1 D(t)$ quantifies the interaction strength with T cells, and the denominator describes inhibition by MSCs. As $D(t)$ increases, the interaction saturates, while an increase in $M(t)$ suppresses this interaction. Although MSCs do not directly inhibit T cell–dendritic cell interactions under normal conditions, during autoimmune responses they modulate these interactions via cytokine-mediated regulatory mechanisms. When $\delta_1 \to 0$, the term reduces to a classical bilinear incidence. This Holling type-II functional form more realistically captures immune saturation effects and prevents unbounded growth in interaction terms. A similar mechanism is modeled by the term $\frac{\gamma_2 T(t)D(t)}{1+\delta_2 M(t)}$. Both terms ultimately contribute to keratinocyte population growth, while $M(t)$ suppresses the T cell–dendritic cell interaction loop and limits infiltration by producing anti-inflammatory cytokines. δ_1 and δ_2 denote the respective scaling coefficients of inhibition. In early stages of disease progression, keratinocytes also suppress T cell over-activation via anti-inflammatory cytokines, modeled by the term $\eta T(t)K(t)$. The per-capita mortality rates for T cells, dendritic cells, keratinocytes, and MSCs are denoted by ρ_T, ρ_D, ρ_K, and ρ_M, respectively. The model parameters are also summarized in Table 1.

Remark 1. Fractional-order systems, in their standard form, often lack dimensional consistency. Indeed, the time dimension on the left-hand side of the Caputo fractional derivative of order λ is $(\text{time})^{-\lambda}$, while the right-hand side of the model (1) carries the dimension $(\text{time})^{-1}$. For the detailed mathematical justification for this dimensional imbal-

Table 1. This table presents the model parameters, their definitions, and the assigned values used in the numerical simulations. Some parameter values are sourced from various literature [13, 18, 24] and some are estimated, which allowed for the biological viability of the model behavior.

Parameter	Definition of parameter	Value (unit)
ξ_T	Constant accumulation rate of T cells in the proximity region	25 $\text{mm}^{-3}d^{-1}$
ξ_D	Constant accumulation rate of dendritic cells in the proximity region	15 $\text{mm}^{-3}d^{-1}$
ξ_K	Constant accumulation rate of keratinocytes in the inflamed area	30 $\text{mm}^{-3}d^{-1}$
ξ_M	Constant accumulation rate of MSCs near the inflamed region	0.5 $\text{mm}^{-3}d^{-1}$
μ	Intrinsic growth rate T cell population	0.03 d^{-1}
$T^{\max}$	Maximum carrying capacity of T cell population	300 mm^{-3}
γ_1	Activation rate of T cells through DC mediated cytokines	0.03 mm^3d^{-1}
γ_2	Rate of activation of DCs via T cell mediated cytokines	0.03 mm^3d^{-1}
δ_1	Inhibition scaling coefficient of MSCs on DC activation	0.035 mm^3
δ_2	Inhibition scaling coefficient of MSCs on T cell activation	0.25 mm^3
η	Initial inhibition rate of T cell hyper-activity by keratinocytes	0.003 mm^3d^{-1}
ρ_T	Natural mortality rate of T cells	0.06 d^{-1}
ρ_D	Natural mortality rate of DCs	0.16 d^{-1}
ρ_K	Inherent mortality rate of keratinocytes	0.25 d^{-1}
ρ_M	Natural mortality rate of MSCs	0.3 d^{-1}

ance and how it can be resolved, we refer to these articles [31, 32]. To address this issue, we introduce a parameter $\mathcal{L}$, referred to as the memory rate parameter, on the left-hand side of the fractional system. This parameter has the dimension of (day^{-1}). To ensure dimensional consistency in model (1), we multiply the left-hand side of each equation by $\mathcal{L}^{1-\lambda}$, yielding $(\text{day}^{-1})^{1-\lambda} \cdot \text{day}^{-\lambda} = \text{day}^{-1}$, which confirms that the model (1) is dimensionally balanced. Similarly, for models (2) and (3), which involve the Caputo–Fabrizio and Atangana–Baleanu fractional derivatives of orders ζ and $\alpha \in (0, 1]$, we apply the same parameter $\mathcal{L}$ to maintain dimensional consistency across all fractional order model formulations. A detailed mathematical derivation demonstrating how $\mathcal{L}$ resolves the dimensional imbalance for Caputo–Fabrizio and Atangana–Baleanu models in the Caputo sense is provided in the Appendix.

5. Positivity and Boundedness

Let us denote $\mathbb{R}^4_+ = \{z(t) \in \mathbb{R}^4 : z(t) > 0\}$ and define the state vector as $z(t) = (T(t), D(t), K(t), M(t))^T$, where ^{T} indicates the transpose. Our objective is to investigate the positivity and to establish the existence of a positively invariant region in which the solutions of the fractional-order model (3), formulated using the Atangana–Baleanu–Caputo (ABC) fractional derivative, reside. This analysis ensures that the model is biologically meaningful and mathematically well-posed throughout the considered time domain.

Now, we state the following theorem, which guarantees the positivity of the solutions of the model (3).

Theorem 2. *If the initial condition satisfies $(T_0, D_0, K_0, M_0)^T$ Int $(\mathbb{R}^4_+)$, then all the solutions of the fractional-order model (3) remain positive for all $t > 0$.*

Proof. Consider the first equation of the fractional-order model (3). Evaluating it at $T = 0$ and $z(t) \in \mathbb{R}^4_+$, we obtain:

$$\mathcal{L}^{1-\alpha}\, {}^{ABC}\mathcal{D}^{\alpha}_t[T(t)]\big|_{T=0,\, z(t)\in\mathbb{R}^4_+} = \xi_T,$$

$$ {}^{ABC}\mathcal{D}^{\alpha}_t[T(t)]\big|_{T=0,\, z(t)\in\mathbb{R}^4_+} = \mathcal{L}^{\alpha-1}\xi_T > 0.$$

In similar manner from the remaining equations of the model (3) one can easily verify

$$ {}^{ABC}\mathcal{D}^{\alpha}_t[D(t)]\big|_{D=0,\, z(t)\in\mathbb{R}^4_+} > 0,$$
$$ {}^{ABC}\mathcal{D}^{\alpha}_t[K(t)]\big|_{K=0,\, z(t)\in\mathbb{R}^4_+} > 0,$$
$$ {}^{ABC}\mathcal{D}^{\alpha}_t[M(t)]\big|_{M=0,\, z(t)\in\mathbb{R}^4_+} > 0.$$

These inequalities confirm that the fractional derivatives of each model variable are strictly positive at the boundary, ensuring that the trajectories point inward at the boundary of the positive octant. Therefore, by the Nagumo condition [33], the solution remains in $\mathbb{R}^4_+$ for all $t > 0$, completing the proof. □

It is also essential to show that the solutions of the fractional-order model (3) remain bounded for all time $t > 0$. The following theorem establishes the invariant region Π, where the solutions of model (3) are biologically feasible and mathematically well-posed.

Suppose $\Pi = \{z(t) \in \mathbb{R}^4 : 0 < T(t) + D(t) + K(t) + M(t) \leq \frac{\kappa}{\rho}\}$. The following theorem confirms that Π is positively invariant for the model (3).

Theorem 3. *The closed set Π is positively invariant with respect to the fractional-order model (3).*

Proof. Let us define the total population as $Y(t) = T(t)+D(t)+K(t)+M(t)$. By adding the equations of the model (3), we obtain the following inequality involving the Atangana–Baleanu–Caputo (ABC) fractional derivative:

$$\mathcal{L}^{1-\alpha}\, {}^{ABC}\mathcal{D}^{\alpha}_t[Y(t)] \leq (\xi_T + \xi_D + \xi_K + \xi_M) + \frac{\mu T^{\max}}{4} - \rho Y(t)$$
$$= \kappa - \rho Y(t),$$

where $\kappa = \xi_T + \xi_D + \xi_K + \xi_M + \frac{\mu T^{\max}}{4}$, and $\rho = \min\{\rho_T, \rho_D, \rho_K, \rho_M\}$. The term $\frac{\mu T^{\max}}{4}$ represents the maximum value of the logistic growth term $\mu T(t)(1 - \frac{T(t)}{T^{\max}})$.

Applying the Laplace transform and using the known identity for the Mittag-Leffler function, the solution $Y(t)$ satisfies:

$$Y(t) \leq Y(0)\,\mathbf{E}_{\alpha}(-\rho\mathcal{L}^{\alpha-1}t^{\alpha}) + \int_0^t \kappa\mathcal{L}^{\alpha-1}\sigma^{\alpha-1}\,\mathbf{E}_{\alpha,\alpha}(-\rho\mathcal{L}^{\alpha-1}\sigma^{\alpha})\,d\sigma.$$

Expanding the Mittag-Leffler function in series and simplifying the integral expression gives:

$$Y(t) \leq Y(0)\,\mathbf{E}_{\alpha}(-\rho\mathcal{L}^{\alpha-1}t^{\alpha}) + \frac{\kappa}{\rho}\left(1-\mathbf{E}_{\alpha}(-\rho\mathcal{L}^{\alpha-1}t^{\alpha})\right).$$

Clearly, if $Y(0) \leq \frac{\kappa}{\rho}$, then for all $t > 0$,

$$0 < Y(t) \leq \frac{\kappa}{\rho} \quad \Rightarrow \quad 0 < T(t)+D(t)+K(t)+M(t) \leq \frac{\kappa}{\rho}.$$

Therefore, it follows that the closed set Π remains positively invariant within the framework of the fractional-order model (3).

□

6. Existence and Uniqueness

In this section, we analyze the existence and uniqueness of solutions to the fractional-order model by employing the Banach contraction mapping principle, corresponding to the Atangana-Baleanu fractional derivative defined in the Caputo sense.

6.1. *Existence of solutions*

We considered our formulated mathematical model (3) and rewritten in the following form:

$$\begin{aligned}
\mathcal{J}_1(t,T,D,K,M) &= \xi_T + \mu T(t)\left[1-\frac{T(t)}{T^{\max}}\right] - \frac{\gamma_1 T(t)D(t)}{1+\delta_1 M(t)} \\
&\quad - \eta T(t)K(t) - \rho_T T(t), \\
\mathcal{J}_2(t,T,D,K,M) &= \xi_D - \frac{\gamma_2 T(t)D(t)}{1+\delta_2 M(t)} - \rho_D D(t), \\
\mathcal{J}_3(t,T,D,K,M) &= \xi_K + \frac{\gamma_1 T(t)D(t)}{1+\delta_1 M(t)} + \frac{\gamma_2 T(t)D(t)}{1+\delta_2 M(t)} \\
&\quad - \rho_K K(t), \\
\mathcal{J}_4(t,T,D,K,M) &= \xi_M - \rho_M M(t).
\end{aligned} \tag{4}$$

Using the eq. (4), the proposed model (3) can be written in the following form:

$$\begin{cases} \mathcal{L}^{1-\alpha}\,{}^{ABC}D_0^{\alpha}\mathcal{H}(t) = \mathcal{J}(t,\mathcal{H}(t)), \quad t\in[0,T],\ 0<\alpha\leq 1, \\ \mathcal{H}(0) = \mathcal{H}_0 > 0. \end{cases} \tag{5}$$

Applying the Lemma 1 on the problem (5), we obtained

$$\mathcal{H}(t) = \mathcal{H}_0(t) + \mathcal{L}^{\alpha-1}[\mathcal{J}(t,\mathcal{H}(t)) - \mathcal{J}_0(t)]\frac{1-\alpha}{\mathbf{B}(\alpha)} + \frac{\alpha\mathcal{L}^{\alpha-1}}{\mathbf{B}(\alpha)\Gamma(\alpha)}\int_0^t (t-s)^{\alpha-1}\mathcal{J}(s,\mathcal{H}(s))ds. \tag{6}$$

where

$$\mathcal{H}(t) = \begin{cases} T(t) \\ D(t) \\ K(t) \\ M(t) \end{cases}, \mathcal{H}_0(t) = \begin{cases} T(0) \\ D(0) \\ K(0) \\ M(0) \end{cases},$$

$$\mathcal{J}(t,\mathcal{H}(t)) = \begin{cases} \mathcal{J}_1(t,T,D,K,M) \\ \mathcal{J}_2(t,T,D,K,M) \\ \mathcal{J}_3(t,T,D,K,M) \\ \mathcal{J}_4(t,T,D,K,M) \end{cases},$$

$$\mathcal{J}_0(t) = \begin{cases} \mathcal{J}_1(0,T,D,K,M) \\ \mathcal{J}_2(0,T,D,K,M) \\ \mathcal{J}_3(0,T,D,K,M) \\ \mathcal{J}_4(0,T,D,K,M) \end{cases}.$$

Now, we prove that all kernels $\mathcal{J}_1, \mathcal{J}_2, \mathcal{J}_3$ and $\mathcal{J}_4$ satisfy the Lipschitz condition. Since all the populations of our system are bounded therefore there exist some positive constants for which we can write all the populations in the form: $u_1 \leq T \leq U_1$, $u_2 \leq D \leq U_2$, $u_3 \leq K \leq U_3$ and $u_4 \leq M \leq U_4$.

First, we prove that the kernel $\mathcal{J}_1$ satisfies the Lipschitz condition. Let $T(t)$ and $T_1(t)$ are two functions, then utilize the norm function properties, we have

$$\begin{aligned}
\|\mathcal{J}_1(t,T(t)) - \mathcal{J}_1(t,T_1(t))\| &= \Big\|\Big(\mu T(t)\Big[1-\frac{T(t)}{T^{\max}}\Big] - \frac{\gamma_1 T(t)D(t)}{1+\delta_1 M(t)} \\
&\quad - \eta T(t)K(t) - \rho_T T(t)\Big) - \Big(\mu T_1(t)\Big[1 \\
&\quad - \frac{T_1(t)}{T^{\max}}\Big] - \frac{\gamma_1 T_1(t)D(t)}{1+\delta_1 M(t)} - \eta T_1(t)K(t) \\
&\quad - \rho_T T_1(t)\Big)\Big\|, \\
&\leq \Big(\mu + \frac{2\mu U_1}{T^{\max}} + \frac{\gamma_1 U_2}{1+\delta_1 u_4} + \eta U_3 \\
&\quad + \rho_T\Big)\|T(t) - T_1(t)\| \\
&= \mathcal{V}_1\|T(t) - T_1(t)\|, \quad \text{where } \mathcal{V}_1 = \Big(\mu \\
&\quad + \frac{2\mu U_1}{T^{\max}} + \frac{\gamma_1 U_2}{1+\delta_1 u_4} + \eta U_3 + \rho_T\Big).
\end{aligned}$$

Similarly, we can prove that the other kernels also satisfy the Lipschitz condition and therefore there exist $\mathcal{V}_2, \mathcal{V}_3, \mathcal{V}_4$ such that

$$\begin{aligned}
\big\|\mathcal{J}_2(t,D(t)) - \mathcal{J}_2(t,D_1(t))\big\| &\leq \mathcal{V}_2\|D(t) - D_1(t)\|, \\
\big\|\mathcal{J}_3(t,K(t)) - \mathcal{J}_3(t,K_1(t))\big\| &\leq \mathcal{V}_3\|K(t) - K_1(t)\|, \\
\big\|\mathcal{J}_4(t,M(t)) - \mathcal{J}_4(t,M_1(t))\big\| &\leq \mathcal{V}_4\|M(t) - M_1(t)\|,
\end{aligned}$$

where

$$\mathcal{V}_2 = \frac{\gamma_1 U_1}{1+\delta_2 u_4} + \rho_D,\ \mathcal{V}_3 = \rho_K, \text{ and } \mathcal{V}_4 = \rho_M.$$

The Lipschitz condition of all kernels in terms of (5) is written in the following lemma:

Lemma 3. *There exists a constant $\mathcal{V}_k > 0$, such that for all $\mathcal{H}_1, \mathcal{H}_2$, the following inequality holds:*

$$\|\mathcal{J}(t, \mathcal{H}_1(t)) - \mathcal{J}(t, \mathcal{H}_2(t))\| \leq \mathcal{V}_k \|\mathcal{H}_1 - \mathcal{H}_2\|.$$

Let $\mathbb{X} = C([0,T];\mathbb{R})$ be the Banach space of all continuous functions from [0, T] to $\mathbb{R}$ defined by

$$\|\mathcal{H}(t)\| = \max_{t\in[0,T]} |\mathcal{H}(t)|,$$

where

$$|\mathcal{H}(t)| = |T(t)| + |D(t)| + |K(t)| + |M(t)|$$
and
$$T, D, K, M \in C([0,T]).$$

From the eq. (6), we consider two operator $\mathcal{X}_1$ and $\mathcal{X}_2$ as

$$\begin{aligned} \mathcal{X}_1(\mathcal{H}) &= \mathcal{H}_0(t) + \mathcal{L}^{\alpha-1}[\mathcal{J}(t,\mathcal{H}(t)) - \mathcal{J}_0(t)]\frac{1-\alpha}{\mathbf{B}(\alpha)}. \\ \mathcal{X}_2(\mathcal{H}) &= \frac{\alpha\mathcal{L}^{\alpha-1}}{\mathbf{B}(\alpha)\Gamma(\alpha)}\int_0^t (t-s)^{\alpha-1}\mathcal{J}(s,\mathcal{H}(s))ds. \end{aligned} \tag{7}$$

Now, we will prove that the operator $\mathcal{X}_1(\mathcal{H})$ is a contraction, and the operator $\mathcal{X}_2(\mathcal{H})$ is compact and continuous. Before proceeding with the proof, we make the following assumption:

(L$_1$) There exist constants κ_1, and κ_2 such that $|\mathcal{J}(t,\mathcal{H})t)| \leq \kappa_1\mathcal{H}(t) + \kappa_2$, where $|\mathcal{H}(t) \leq m|$.

First, we prove that $\mathcal{X}_1(\mathcal{H})$ is a contraction using the Banach contraction principle. Let $\mathcal{H}_1 \in \mathbb{X}$ and $\mathcal{H}_2 \in \mathbb{X}$. By applying the Lemma 3 to the operator $\mathcal{X}_1$, as defined in the eq. (7), we have:

$$\begin{aligned} \|\mathcal{X}_1(\mathcal{H}_1) - \mathcal{X}_1(\mathcal{H}_2)\| &= \mathcal{L}^{\alpha-1}\frac{1-\alpha}{\mathbf{B}(\alpha)} \times \max_{t\in(0,T)} |\mathcal{J}(t,\mathcal{H}_1(t) \\ &\quad - \mathcal{J}(t,\mathcal{H}_2(t))| \\ &\leq \mathcal{L}^{\alpha-1}\frac{(1-\alpha)\mathcal{V}_k}{\mathbf{B}(\alpha)}\|\mathcal{H}_1 - \mathcal{H}_2\|. \end{aligned}$$

This implies that the operator $\mathcal{X}_1(\mathcal{H})$ is a contraction. Next, we prove that the other operator, $\mathcal{X}_2(\mathcal{H})$, is compact.

$$\begin{aligned} |\mathcal{X}_2(\mathcal{H})| &= \max_{t\in(0,T)} \frac{\alpha\mathcal{L}^{\alpha-1}}{\mathbf{B}(\alpha)\Gamma(\alpha)} \times \left\| \int_0^t (t-s)^{\alpha-1}\mathcal{J}(s,\mathcal{H}(s))ds \right\| \\ &\leq \frac{\alpha\mathcal{L}^{\alpha-1}}{\mathbf{B}(\alpha)\Gamma(\alpha)} \int_0^T (t-s)^{\alpha-1}\Big|\mathcal{J}(s,\mathcal{H}(s))\Big|ds \\ &\leq \frac{T^\alpha\mathcal{L}^{\alpha-1}}{\mathbf{B}(\alpha)\Gamma(\alpha)}[\kappa_1 m + \kappa_2]. \end{aligned}$$

Therefore, the operator $\mathcal{X}_2(\mathcal{H})$ is bounded. Next, we need to prove that the operator is continuous. To do so, let us assume that $t_1, t_2 \in [0,T]$, where $t_2 > t_1$.

$$\begin{aligned} |\mathcal{X}_2(\mathcal{H}(t_2)) - \mathcal{X}_2(\mathcal{H}(t_1))| &= \frac{\alpha\mathcal{L}^{\alpha-1}}{\mathbf{B}(\alpha)\Gamma(\alpha)}\left| \int_0^{t_2} (t_2-s)^{\alpha-1}\mathcal{J}(s,\mathcal{H}(s))ds \right. \\ &\quad \left. - \int_0^{t_1} (t_1-s)^{\alpha-1}\mathcal{J}(s,\mathcal{H}(s))ds \right| \\ &\leq \mathcal{L}^{\alpha-1}\frac{[\kappa_1 m + \kappa_2]}{\mathbf{B}(\alpha)\Gamma(\alpha)}\left[t_2^\alpha - t_1^\alpha\right]. \end{aligned}$$

This implies that $|\mathcal{X}_2(\mathcal{H}(t_2)) - \mathcal{X}_2(\mathcal{H}(t_1))| \to 0$ as $t_2 \to t_1$. Therefore, the operator $\mathcal{X}_2(\mathcal{H})$ is compact. Since the operator $\mathcal{X}_1(\mathcal{H})$ is a contraction and the operator $\mathcal{X}_2(\mathcal{H})$ is compact, it follows from Theorem 1 that the eq. (6) has one or more solutions. In the subsequent section, we will prove that the solution is unique.

6.2. Uniqueness of Solutions

Theorem 4. *The integral problem (5), together with Lemma 3, admits a unique solution if the following condition is satisfied:*

$$\mathcal{L}^{\alpha-1}\left[\frac{(1-\alpha)\mathcal{V}_k}{\mathbf{B}(\alpha)} + \frac{T^\alpha\mathcal{V}_k}{\mathbf{B}(\alpha)\Gamma(\alpha)}\right] < 1. \tag{8}$$

Consequently, the solution of the fractional model (3) is also unique under the condition (8).

Proof. Let $\Psi : \mathbb{X} \to \mathbb{X}$ be the operator defined by

$$\begin{aligned} \Psi(\mathcal{H}(t)) &= \mathcal{H}_0(t) + \mathcal{L}^{\alpha-1}\left[\mathcal{J}(t,\mathcal{H}(t)) - \mathcal{J}_0(t)\right]\frac{1-\alpha}{\mathbf{B}(\alpha)} \\ &\quad + \frac{\alpha\mathcal{L}^{\alpha-1}}{\mathbf{B}(\alpha)\Gamma(\alpha)}\int_0^t (t-s)^{\alpha-1}\mathcal{J}(s,\mathcal{H}(s))\,ds. \end{aligned}$$

Now, consider two functions $\mathcal{H}_1, \mathcal{H}_2 \in \mathbb{X}$. Then,

$$\begin{aligned} \|\Psi(\mathcal{H}_1(t)) - \Psi(\mathcal{H}_2(t))\| &\leq \mathcal{L}^{\alpha-1}\cdot\frac{1-\alpha}{\mathbf{B}(\alpha)}\cdot\max_{t\in[0,T]}\Big|\mathcal{J}(t,\mathcal{H}_1(t)) \\ &\quad - \mathcal{J}(t,\mathcal{H}_2(t))\Big| + \frac{\alpha\mathcal{L}^{\alpha-1}}{\mathbf{B}(\alpha)\Gamma(\alpha)}\cdot\max_{t\in[0,T]}\left|\int_0^t (t \\ &\quad - s)^{\alpha-1}\left[\mathcal{J}(s,\mathcal{H}_1(s)) - \mathcal{J}(s,\mathcal{H}_2(s))\right]ds\right| \\ &\leq \mathcal{L}^{\alpha-1}\left[\frac{(1-\alpha)\mathcal{V}_k}{\mathbf{B}(\alpha)} + \frac{T^\alpha\mathcal{V}_k}{\mathbf{B}(\alpha)\Gamma(\alpha)}\right]\cdot\|\mathcal{H}_1 - \mathcal{H}_2\| \\ &= \Lambda\cdot\|\mathcal{H}_1 - \mathcal{H}_2\|. \end{aligned}$$

Therefore, by the Banach contraction principle, Ψ is a contraction mapping if $\Lambda < 1$. Hence, by the fixed-point theorem, the fractional model (3) admits a unique solution under the condition $\Lambda < 1$.

Remark 2. When $\Lambda \geq 1$, the operator $\Psi : \mathbb{X} \to \mathbb{X}$ is no longer a contraction mapping, i.e., the distance property $d(\Psi(x),\Psi(y)) < d(x,y)$ is lost. If Λ=1, the distance property of the operator is preserved or reduced, but not strictly reduced, which means the uniqueness of a fixed point is not guaranteed, and solutions may be non-unique or not necessarily approachable by standard iterations. Whenever $\Lambda > 1$, the operator increases distances between two points, implying that the iterative sequence would diverge. Therefore, for $\Lambda \geq 1$, the model is invalid for biological interpretation.

□

Biological Interpretation: The existence and uniqueness of solutions in a fractional model ensure that the biological system exhibits a consistent and predictable response during treatment.

Existence guarantees that a meaningful outcome occurs under given conditions, while uniqueness confirms the reproducibility of this response. The fractional aspect captures memory effects in biological processes, reflecting the influence of past therapeutic interventions. This enhances the model's reliability in representing the dynamics of the immune response.

7. Stability Analysis

In this section, we present the stability analysis for our fractional model (3) in the context of Ulam-Hyers stability and generalized Ulam-Hyers stability. The concept of Ulam-Hyers stability, introduced by Ulam in [34], provides a framework for analyzing the robustness of solutions to perturbations in functional equations. Before presenting the proof of the system's stability, we introduce some definitions that will be utilized in the subsequent stability analysis. Let $\epsilon > 0$ and $h : [0,T] \to [0,\infty)$ be a continuous function. We consider the following inequalities.

$$|\mathcal{L}^{1-\alpha}\, {}^{ABC}D^{\alpha}_{0+}\mathcal{H}(t) - \mathcal{J}(t,\mathcal{H}(t))| \le \epsilon, \quad t \in [0,T], \tag{9}$$

$$|\mathcal{L}^{1-\alpha}\, {}^{ABC}D^{\alpha}_{0+}\mathcal{H}(t) - \mathcal{J}(t,\mathcal{H}(t))| \le \epsilon h(t), \quad t \in [0,T]. \tag{10}$$

Definition 5. The solutions of the proposed mathematical model (3) are said to be **Ulam-Hyers stable** if, for every $\epsilon > 0$ and for a function $\bar{\mathcal{H}} \in \mathbb{X}$ satisfying the inequality (9), there exists a solution $\mathcal{H}(t)$ of model (3) such that

$$|\bar{\mathcal{H}}(t) - \mathcal{H}(t)| < \mathcal{N}_k\epsilon, \quad t \in [0,T], \tag{11}$$

where $\mathcal{N}_k$ is a positive constant.

Definition 6. The solutions of the model (3) are said to be **generalized Ulam–Hyers stable** if there exists a continuous function $\Phi_k : \mathbb{R}_+ \to \mathbb{R}_+$ with $\Phi_k(0) = 0$, such that for arbitrary $\epsilon > 0$ and for each $\bar{\mathcal{H}} \in \mathbb{X}$ satisfying the inequality (10), there exists a solution $\mathcal{H} \in \mathbb{X}$ of the model (3) such that

$$|\bar{\mathcal{H}}(t) - \mathcal{H}(t)| < \Phi_k\epsilon, \quad t \in [0,T]. \tag{12}$$

Remark 3. We aim to analyze the stability of the proposed model (3). A function $\mathcal{H} \in \mathbb{X}$ satisfies the inequality (9) if and only if there exists a perturbation function $g \in \mathbb{X}$ such that the following conditions hold:

(i) $|g(t)| \le \epsilon, \quad t \in [0,T]$,

(ii) $\mathcal{L}^{1-\alpha}\, {}^{ABC}D^{\alpha}_{0+}\mathcal{H}(t) = \mathcal{J}(t,\mathcal{H}(t)) + g(t), \quad t \in [0,T]$.

Theorem 5. *Let $\mathcal{H} \in \mathbb{X}$ satisfy the inequality (9) and the properties described in Remark 3. Then $\mathcal{H}$ satisfies the following inequality:*

$$\Omega\epsilon \ge \left|\mathcal{H}(t) - \left(\mathcal{H}_0 + \frac{\mathcal{L}^{\alpha-1}(1-\alpha)}{\mathbf{B}(\alpha)}\Big[\mathcal{J}(t,\mathcal{H}(t)) - \mathcal{J}_0(t)\Big] + \frac{\mathcal{L}^{\alpha-1}\alpha}{\mathbf{B}(\alpha)\Gamma(\alpha)}\int_0^t \mathcal{J}(s,\mathcal{H}(s))(t-s)^{\alpha-1}ds\right)\right|,$$

where

$$\Omega = \frac{\mathcal{L}^{\alpha-1}\left(\Gamma(\alpha)(1-\alpha) + T^{\alpha}\right)}{\mathbf{B}(\alpha)\Gamma(\alpha)}.$$

Proof. Considering the second part of the Remark 3 and applying the theorem in [35], we obtained

$$\begin{aligned}\mathcal{H}(t) = \mathcal{H}_0 &+ \frac{\mathcal{L}^{\alpha-1}(1-\alpha)}{\mathbf{B}(\alpha)}\Big[\mathcal{J}(t,\mathcal{H}(t)) - \mathcal{J}_0(t)\Big] \\ &+ \frac{\mathcal{L}^{\alpha-1}\alpha}{\mathbf{B}(\alpha)\Gamma(\alpha)}\int_0^t \mathcal{J}(s,\mathcal{H}(s))(t-s)^{\alpha-1}ds \\ &+ \frac{\mathcal{L}^{\alpha-1}(1-\alpha)}{\mathbf{B}(\alpha)}g(t) + \frac{\mathcal{L}^{\alpha-1}\alpha}{\mathbf{B}(\alpha)\Gamma(\alpha)}\int_0^t g(s)(t-s)^{\alpha-1}ds.\end{aligned}$$

Using the first of Remark 3, we get

$$\begin{aligned}\varkappa &\le \frac{\mathcal{L}^{\alpha-1}(1-\alpha)}{\mathbf{B}(\alpha)}|g(t)| + \frac{\mathcal{L}^{\alpha-1}\alpha}{\mathbf{B}(\alpha)\Gamma(\alpha)}\int_0^t (t-s)^{\alpha-1}|g(s)|ds \\ &\le \frac{\mathcal{L}^{\alpha-1}(1-\alpha)}{\mathbf{B}(\alpha)}\epsilon + \frac{\mathcal{L}^{\alpha-1}T^{\alpha}}{\mathbf{B}(\alpha)\Gamma(\alpha)}\epsilon, \\ &= \Omega\epsilon,\end{aligned}$$

where

$$\varkappa = \left|\mathcal{H}(t) - \left(\mathcal{H}_0 + \frac{\mathcal{L}^{\alpha-1}(1-\alpha)}{\mathbf{B}(\alpha)}\Big[\mathcal{J}(t,\mathcal{H}(t)) - \mathcal{J}_0(t)\Big] + \frac{\mathcal{L}^{\alpha-1}\alpha}{\mathbf{B}(\alpha)\Gamma(\alpha)}\int_0^t \mathcal{J}(s,\mathcal{H}(s))(t-s)^{\alpha-1}ds\right)\right|.$$

□

Theorem 6. *Suppose that $\mathcal{J} : [0,T]\times\mathbb{R}^4 \to \mathbb{R}$ is continuous for every $\mathcal{H} \in \mathbb{X}$ and our assumption (L_1) are satisfied with condition $1-\Lambda > 0$. Then our proposed fractional model (3) is Ulam-Hyers stable and also generalized Ulam-Hyers stable. Where*

$$\Lambda = \mathcal{L}^{\alpha-1}\left[\frac{(1-\alpha)\mathcal{V}_k}{\mathbf{B}(\alpha)} + \frac{T^{\alpha}\mathcal{V}_k}{\mathbf{B}(\alpha)\Gamma(\alpha)}\right].$$

Proof. Suppose that $\mathcal{H} \in \mathbb{X}$ be the solution satisfies the inequality (9) and $\mathcal{H}_1 \in \mathbb{X}$ be the unique solution of the model (3). Then

$$\left|\mathcal{H}(t) - \mathcal{H}_1(t)\right| = \left|\mathcal{H}(t) - \left(\mathcal{H}_0 + \frac{\mathcal{L}^{\alpha-1}(1-\alpha)}{\mathbf{B}(\alpha)}\Big[\mathcal{J}(t,\mathcal{H}_1(t)) - \mathcal{J}_0(t)\Big] + \frac{\mathcal{L}^{\alpha-1}\alpha}{\mathbf{B}(\alpha)\Gamma(\alpha)}\int_0^t \mathcal{J}(s,\mathcal{H}_1(s))(t-s)^{\alpha-1}ds\right)\right|,$$

$$
\begin{aligned}
&\leq \Bigg|\mathcal{H}(t) - \Bigg(\mathcal{H}_0 + \frac{\mathcal{L}^{\alpha-1}(1-\alpha)}{\mathbf{B}(\alpha)}\Big[\mathcal{J}(t,\mathcal{H}(t)) - \mathcal{J}_0(t)\Big] \\
&\quad + \frac{\mathcal{L}^{\alpha-1}\alpha}{\mathbf{B}(\alpha)\Gamma(\alpha)}\int_0^t \mathcal{J}(s,\mathcal{H}(s))(t-s)^{\alpha-1}ds\Bigg)\Bigg| \\
&\quad + \Bigg|\Bigg(\mathcal{H}_0 + \frac{\mathcal{L}^{\alpha-1}(1-\alpha)}{\mathbf{B}(\alpha)}\Big[\mathcal{J}(t,\mathcal{H}(t)) - \mathcal{J}_0(t)\Big] \\
&\quad + \frac{\mathcal{L}^{\alpha-1}\alpha}{\mathbf{B}(\alpha)\Gamma(\alpha)}\int_0^t \mathcal{J}(s,\mathcal{H}(s))(t-s)^{\alpha-1}ds\Bigg) \\
&\quad - \Bigg(\mathcal{H}_0 + \frac{\mathcal{L}^{\alpha-1}(1-\alpha)}{\mathbf{B}(\alpha)}\Big[\mathcal{J}(t,\mathcal{H}_1(t)) - \mathcal{J}_0(t)\Big] \\
&\quad + \frac{\mathcal{L}^{\alpha-1}\alpha}{\mathbf{B}(\alpha)\Gamma(\alpha)}\int_0^t \mathcal{J}(s,\mathcal{H}_1(s))(t-s)^{\alpha-1}ds\Bigg)\Bigg|, \\
&\leq \Omega\epsilon + \frac{\mathcal{L}^{\alpha-1}(1-\alpha)}{\mathbf{B}(\alpha)}\mathcal{V}_k|\mathcal{H}(t) - \mathcal{H}_1(t)| \\
&\quad + \mathcal{L}^{\alpha-1}\frac{T^\alpha \mathcal{V}_k}{\mathbf{B}(\alpha)\Gamma(\alpha)}|\mathcal{H}(t) - \mathcal{H}_1(t)|, \\
&= \Omega\epsilon + \Lambda|\mathcal{H}(t) - \mathcal{H}_1(t)|.
\end{aligned}
$$

Hence, $|\mathcal{H}(t) - \mathcal{H}_1(t)| \leq \mathcal{N}_k\epsilon$, where $\mathcal{N}_k = \frac{\Omega}{1-\Lambda}$.

Here we consider $\Phi_k(\epsilon) = \mathcal{N}_k\epsilon$ such that $\Phi_k(0) = 0$. So we conclude the the model (3) is Ulam-Hyers stable as well as generalized Ulam-Hyers stable. □

Biological Significance: The generalized Ulam-Hyers stability signifies that under small perturbations or uncertainties characteristic in biological processes, such as minor fluctuations in stem cell proliferation rates or therapeutic interventions, the system's trajectory, representing the progression or degradation of psoriasis, remains close to its ideal and equilibrium state. This mathematical robustness suggests that the disease dynamics are not excessively sensitive to minor biological noise, and that therapeutic strategies aiming to shift the system to a stable equilibrium are likely to be effective and maintainable in a real-world, dynamic biological environment.

8. Fractional Order control problem

In the case of psoriasis, the interaction rates between T cells and dendritic cells are highly stimulated by the effects of the cytokines TNF-α and IL-23, which result in the abnormal differentiation of T cells and hyper-proliferation of keratinocytes. To control the effects of these cytokines, we have considered our model by introducing two control functions, namely, $u_1(t)$ and $u_2(t)$ $(j = 1, 2)$ which are permissible controls representing the effect of biologics TNF-α inhibitors and IL-23 blockers respectively in order to restrict the interaction rates γ_1 and γ_2, respectively. Therefore, models (1) to (3) equipped with optimum controls is given by the following system of equations specified in the time interval $[0, t_f]$.

$$
\begin{aligned}
{}^{\mathcal{L}^{(1-a)F}}D_t^a[T(t)] &= \xi_T + \mu T(t)\left[1 - \frac{T(t)}{T^{\max}}\right] - \eta T(t)K(t) \\
&\quad - \frac{\gamma_1\big[1-u_1(t)\big]T(t)D(t)}{1+\delta_1 M(t)} - \rho_T T(t), \\
{}^{\mathcal{L}^{(1-a)F}}D_t^a[D(t)] &= \xi_D - \frac{\gamma_2\big[1-u_2(t)\big]T(t)D(t)}{1+\delta_2 M(t)} - \rho_D D(t), \\
{}^{\mathcal{L}^{(1-a)F}}D_t^a[K(t)] &= \xi_K + \frac{\gamma_1\big[1-u_1(t)\big]T(t)D(t)}{1+\delta_1 M(t)} \\
&\quad + \frac{\gamma_2\big[1-u_2(t)\big]T(t)D(t)}{1+\delta_2 M(t)} - \rho_K K(t), \\
{}^{\mathcal{L}^{(1-a)F}}D_t^a[M(t)] &= \xi_M - \rho_M M(t),
\end{aligned}
\tag{14}
$$

subject to the initial conditions:

$$
\begin{aligned}
&T(0) = T_0 > 0,\ D(0) = D_0 > 0,\ K(0) = K_0 > 0, \\
&M(0) = M_0 > 0.
\end{aligned}
$$

Note that we do not specify a particular fractional operator at this stage, as our objective is to simulate the fractional-order control system using all three considered fractional operators for comparative analysis.

In the following subsection we explain the solution of the above mentioned control induced system with respect to three different fractional operators with different kernels. For this we have written the three fractional system in a vector notation in general form as:

$$
{}^{\mathcal{L}^{(1-a)F}}D_t^a\big(X_i(t)\big) = \psi\big(X_i(t), u_j(t)\big)\ \ \big[i = 1,2,3,4 \text{ and } j = 1,2\big].
$$

Where 'F' symbolized the three different fractional operators and 'a' is the order of the corresponding method. $\psi\big(X_i(t), u_j\big)$ denotes the right hand side of each fractional order control system.

8.1. The description of Objective functional :

Here, we construct an objective cost functional in order to minimizing the effect of two key inflammatory cytokines, TNF-α and IL-23, which are associated to the interactions between T cells and dendritic cells simultaneously, reducing the related cost of these biologic treatments. For this, we use two control measures: (i) a TNF-α inhibitor and (ii) an IL-23 blocker those inhibit the effects of the cytokine TNF-α and IL-23. Thus, our considered cost functional takes the form:

$$
\text{Minimize}\ \ Z(u_1,u_2) = {}_0I_{t_f}^a\big[K^2(t) + \mathcal{P}_1 u_1^2(t) + \mathcal{P}_2 u_2^2(t)\big]. \tag{15}
$$

subject to the optimal control-induced model (14) along with the specified initial conditions. Here, ${}_0I_{t_f}^a$ denotes the fractional integral operator. The terms $\mathcal{P}_1$ and $\mathcal{P}_2$ represent the positive weight constants associated with the control functions $u_1(t)$ and $u_2(t)$, respectively, and the units of $\mathcal{P}_1$ and $\mathcal{P}_2$ are the same as $K^2(t)$. We used a quadratic cost functional to measure cost in the control problem, since it fits the nonlinearity and it also prevents the bang-bang or singular optimal control cases [36]. The control set is defined over the time interval $[0, t_f]$, where t_f denotes the total duration of control implementation. The admissible set of Lebesgue measurable controls is given by:

$$
U = \big\{\big(u_1(t), u_2(t)\big) :\ 0 < u_j(t) < 1,\ (j = 1,2),\ t \in [0, t_f]\big\}.
$$

The aim of the optimum control problem is to determine the optimal control functions for the model (14), represented by $u_j^*(t)$ where $j = 1, 2$.

$$
Z\big[u_1^*(t), u_2^*(t)\big] = \min\big\{Z(u_1(t), u_2(t)) : u_j(t) \in U, (j = 1,2)\big\}. \tag{16}
$$

Applying the fractional optimality conditions based on Pontryagin's Minimum principle [37] we state and prove the following theorem and determine the conditions for solving this optimum control problem for the control induced model (14).

Theorem 7. *Suppose $\mathcal{T}, \mathcal{D}, \mathcal{K}, \mathcal{M}$ be the optimal state solutions for the fractional order model (14) associated with the optimal controls u_1^*, u_2^* which minimizes the cost functional (15) over admissible control set U. then there exist adjoint variables θ_i $(i = 1, 2, 3, 4)$ satisfying*

$$\begin{aligned}
\mathcal{L}^{(1-a)}\,{}^{F}D_t^a[\theta_1(t')] =& -\theta_1\Big[\mu\Big(1-\frac{2T}{T^{\max}}\Big)-\frac{\gamma_1(1-u_1)D}{1+\delta_1 M}\\
&-\eta K-\rho_T\Big]+\theta_2\Big[\frac{\gamma_2(1-u_2)D}{1+\delta_2 M}\Big]\\
&-\theta_3\Big[\frac{\gamma_1(1-u_1)D}{1+\delta_1 M}+\frac{\gamma_2(1-u_2)D}{1+\delta_2 M}\Big],\\
\mathcal{L}^{(1-a)}\,{}^{F}D_t^a[\theta_2(t')] =& \theta_1\Big[\frac{\gamma_1(1-u_1)T}{1+\delta_1 M}\Big]+\theta_2\Big[\frac{\gamma_2(1-u_2)T}{1+\delta_2 M}\\
&+\rho_D\Big]-\theta_3\Big[\frac{\gamma_1(1-u_1)T}{1+\delta_1 M}\\
&+\frac{\gamma_2(1-u_2)T}{1+\delta_2 M}\Big],\\
\mathcal{L}^{(1-a)}\,{}^{F}D_t^a[\theta_3(t')] =& -2K+\theta_1\big[\eta T\big]+\theta_3\big[\rho_K\big],\\
\mathcal{L}^{(1-a)}\,{}^{F}D_t^a[\theta_4(t')] =& -\theta_1\Big[\frac{\delta_1\gamma_1(1-u_1)TD}{(1+\delta_1 M)^2}\Big]+\theta_4\Big[\rho_M\Big]\\
&-\theta_2\Big[\frac{\delta_2\gamma_2(1-u_2)TD}{(1+\delta_2 M)^2}\Big]\\
&+\theta_3\Big[\frac{\delta_1\gamma_1(1-u_1)TD}{(1+\delta_1 M)^2}\\
&+\frac{\delta_2\gamma_2(1-u_2)T\mathcal{D}}{(1+\delta_2 M)^2}\Big].
\end{aligned}$$

where $t' = t_f - t$ with the transversality conditions

$$\theta_1(t_f) = \theta_2(t_f) = \theta_3(t_f) = \theta_4(t_f) = 0.$$

Furthermore, optimal solutions (u_1^*, u_2^*) that minimizes the fractional optimal control in U, are given by:

$$\begin{aligned}
u_1^*(t) &= \max\Big[0, \min\Big\{1, \frac{(\theta_3-\theta_1)(\gamma_1\mathcal{TD})}{2\mathcal{P}_1(1+\delta_1\mathcal{M})}\Big\}\Big],\\
u_2^*(t) &= \max\Big[0, \min\Big\{1, \frac{(\theta_3-\theta_2)(\gamma_2\mathcal{TD})}{2\mathcal{P}_2(1+\delta_2\mathcal{M})}\Big\}\Big].
\end{aligned} \tag{17}$$

Proof. To characterize the optimal control, we apply Pontryagin's Minimum Principle, we define the Hamiltonian function $H(T, D, K, M, \theta_i, u_j, t)$ as following:

$$\begin{aligned}
H = K^2 &+ \mathcal{P}_1 u_1^2 + \mathcal{P}_2 u_2^2 + \theta_1\mathcal{L}^{(a-1)}\Big[\xi_T + \mu T\Big(1-\frac{T}{T^{\max}}\Big)\\
&-\frac{\gamma_1(1-u_1)TD}{1+\delta_1 M}-\eta TK-\rho_T T\Big]+\theta_2\mathcal{L}^{(a-1)}\Big[\xi_D\\
&-\frac{\gamma_2(1-u_2)TD}{1+\delta_2 M}-\rho_D D\Big]+\theta_3\mathcal{L}^{(a-1)}\Big[\xi_K\\
&+\frac{\gamma_1(1-u_1)TD}{1+\delta_1 M}+\frac{\gamma_2(1-u_2)TD}{1+\delta_2 M}\\
&-\rho_K K\Big]+\theta_4\mathcal{L}^{(a-1)}\Big[\xi_M-\rho_M M\Big],
\end{aligned} \tag{18}$$

where $\theta_i(t)$'s $(i = 1, 2, 3, 4)$ are the adjoint variables obtained by using right fractional derivative of the eq. (18) over $[0, t_f]$ with respect to optimal state variables $\mathcal{T}, \mathcal{D}, \mathcal{K}, \mathcal{M}$ that satisfy:

$$\begin{aligned}
\mathcal{L}^{(1-a)}\,{}^{F}_{t}D^a_{t_f}[\theta_1(t)] =& -\frac{\partial H(T,D,K,M,\theta_i,u_j^*,t)}{\partial T}\\
=& -\theta_1\Big[\mu\Big(1-\frac{2T}{T^{\max}}\Big)-\frac{\gamma_1(1-u_1)D}{1+\delta_1 M}\\
&-\eta K-\rho_T\Big]+\theta_2\Big[\frac{\gamma_2(1-u_2)D}{1+\delta_2 M}\Big]\\
&-\theta_3\Big[\frac{\gamma_1(1-u_1)D}{1+\delta_1 M}+\frac{\gamma_2(1-u_2)D}{1+\delta_2 M}\Big],\\
\mathcal{L}^{(1-a)}\,{}^{F}_{t}D^a_{t_f}[\theta_2(t)] =& -\frac{\partial H(T,D,K,M,\theta_i,u_j^*,t)}{\partial D}\\
=& \theta_1\Big[\frac{\gamma_1(1-u_1)T}{1+\delta_1 M}\Big]+\theta_2\Big[\frac{\gamma_2(1-u_2)T}{1+\delta_2 M}\\
&+\rho_D\Big]-\theta_3\Big[\frac{\gamma_1(1-u_1)T}{1+\delta_1 M}+\frac{\gamma_2(1-u_2)T}{1+\delta_2 M}\Big],\\
\mathcal{L}^{(1-a)}\,{}^{F}_{t}D^a_{t_f}[\theta_3(t)] =& -\frac{\partial H(T,D,K,M,\theta_i,u_j^*,t)}{\partial K}\\
=& -2K+\theta_1\big[\eta T\big]+\theta_3\big[\rho_K\big],\\
\mathcal{L}^{(1-a)}\,{}^{F}_{t}D^a_{t_f}[\theta_4(t)] =& -\frac{\partial H(T,D,K,M,\theta_i,u_j^*,t)}{\partial M}\\
=& -\theta_1\Big[\frac{\delta_1\gamma_1(1-u_1)TD}{(1+\delta_1 M)^2}\Big]\\
&-\theta_2\Big[\frac{\delta_2\gamma_2(1-u_2)TD}{(1+\delta_2 M)^2}\Big]\\
&+\theta_3\Big[\frac{\delta_1\gamma_1(1-u_1)TD}{(1+\delta_1 M)^2}\\
&+\frac{\delta_2\gamma_2(1-u_2)TD}{(1+\delta_2 M)^2}\Big]+\theta_4\Big[\rho_M\Big].
\end{aligned} \tag{19}$$

According to Lemma 2, the adjoint system can be equivalently expressed using the left-sided fractional derivative as follows:

$$\begin{aligned}
\mathcal{L}^{(1-a)}\,{}^{F}_{0}D^a_{t}[\theta_1(t')] =& -\theta_1(t')\Big[-\frac{\gamma_1(1-u_1(t'))D(t')}{1+\delta_1 M(t')}-\eta K\\
&-\rho_T+\mu\Big(1-\frac{2T(t')}{T^{\max}}\Big)\Big]\\
&+\theta_2(t')\Big[\frac{\gamma_2(1-u_2(t'))D(t')}{1+\delta_2 M(t')}\Big]\\
&-\theta_3(t')\Big[\frac{\gamma_1(1-u_1(t'))D(t')}{1+\delta_1 M(t')}\\
&+\frac{\gamma_2(1-u_2(t'))D(t')}{1+\delta_2 M(t')}\Big],\\
\mathcal{L}^{(1-a)}\,{}^{F}_{0}D^a_{t}[\theta_2(t')] =& \theta_1(t')\Big[\frac{\gamma_1(1-u_1(t'))T(t')}{1+\delta_1 M(t')}\Big]
\end{aligned}$$

$$
\begin{aligned}
&+\theta_2(t')\Big[\frac{\gamma_2(1-u_2(t'))T(t')}{1+\delta_2 M(t')}+\rho_D\Big]\\
&-\theta_3(t')\Big[\frac{\gamma_1(1-u_1(t'))T(t')}{1+\delta_1 M(t')}\\
&+\frac{\gamma_2(1-u_2(t'))T(t')}{1+\delta_2 M(t')}\Big],\\
\mathcal{L}^{(1-a)}{}_0^F D_t^a[\theta_3(t')] =\ &-2K(t')+\theta_1(t')\big[\eta T\big]+\theta_3(t')\big[\rho_K\big],\\
\mathcal{L}^{(1-a)}{}_0^F D_t^a[\theta_4(t')] =\ &-\theta_1(t')\Big[\frac{\delta_1\gamma_1(1-u_1(t'))T(t')D(t')}{(1+\delta_1 M(t'))^2}\Big]\\
&-\theta_2(t')\Big[\frac{\delta_2\gamma_2(1-u_2(t'))T(t')D(t')}{(1+\delta_2 M(t'))^2}\Big]\\
&+\theta_3(t')\Big[\frac{\delta_1\gamma_1(1-u_1(t'))T(t')D(t')}{(1+\delta_1 M(t'))^2}\\
&+\frac{\delta_2\gamma_2(1-u_2(t'))T(t')D(t')}{(1+\delta_2 M(t'))^2}\Big]\\
&+\theta_4(t')\Big[\rho_M\Big],
\end{aligned}
\tag{20}
$$

where $t'=t_f-t$.

Here ${}^F D^a$ denotes the arbitrary fractional differential operator. Since, it is very vast to incorporate considered differential operators into this control problem, we solve and compare with different kernels by numerical simulations. In order to determine the optimal controls $u_1^*(t)$ and $u_2^*(t)$ using the first order necessary condition for optimality provided by

$$
\left.\frac{\partial H}{\partial u_1}\right|_{(\mathcal{T},\mathcal{D},\mathcal{K},\mathcal{M},\theta_i,u_j^*,t)} = 0 = \left.\frac{\partial H}{\partial u_2}\right|_{(\mathcal{T},\mathcal{D},\mathcal{K},\mathcal{M},\theta_i,u_j^*,t)}. \tag{21}
$$

Thus, utilizing the above-mentioned eq. (21), we have

$$
u_1^*(t)=\frac{(\theta_3-\theta_1)(\gamma_1\mathcal{TD})}{2\mathcal{P}_1(1+\delta_1\mathcal{M})} \text{ and } u_2^*(t)=\frac{(\theta_3-\theta_2)(\gamma_2\mathcal{TD})}{2\mathcal{P}_2(1+\delta_2\mathcal{M})}.
$$

To ensure that the control functions u_1^* and u_2^* represent optimal solutions, the second-order sufficient conditions for a minima must be satisfied. Specifically, the Hamiltonian H must fulfill:

$$
\left.\frac{\partial^2 H}{\partial u_i^2}\right|_{u_i=u_i^*}>0, \quad \text{for } i=1,2.
$$

For the present problem, we obtain:

$$
\left.\frac{\partial^2 H}{\partial u_i^2}\right|_{u_i=u_i^*}=2\mathcal{P}_i>0, \quad \text{for } i=1,2,
$$

which confirms that u_i^* minimizes the Hamiltonian and satisfies the second-order condition under Pontryagin's Minimum Principle.

The conventional control's boundedness criterion and the characteristics of the control set U, we have the compact form of control profiles i.e., the eq. (17). □

8.2. FBSM-Based Numerical Schemes for Different Fractional Operators

Let us take the state variables of the control system $X_1(t)=T(t), X_2(t)=D(t), X_3(t)=K(t)$, and $X_4(t)=M(t)$. We have also considered the functions $f_i(i=1,2,3,4)$ as:

$$
\begin{aligned}
f_1(t) &= \mathcal{L}^{(a-1)}\Big[\xi_T+\mu T(t)\Big[1-\frac{T(t)}{T^{\max}}\Big]-\eta T(t)K(t)-\rho_T T(t)\\
&\quad -\frac{\gamma_1\big[1-u_1(t)\big]T(t)D(t)}{1+\delta_1 M(t)}\Big],\\
f_2(t) &= \mathcal{L}^{(a-1)}\Big[\xi_D-\frac{\gamma_2\big[1-u_2(t)\big]T(t)D(t)}{1+\delta_2 M(t)}-\rho_D D(t)\Big],\\
f_3(t) &= \mathcal{L}^{(a-1)}\Big[\xi_K+\frac{\gamma_1\big[1-u_1(t)\big]T(t)D(t)}{1+\delta_1 M(t)}-\rho_K K(t)\\
&\quad +\frac{\gamma_2\big[1-u_2(t)\big]T(t)D(t)}{1+\delta_2 M(t)}\Big],\\
f_4(t) &= \mathcal{L}^{(a-1)}\Big[\xi_M-\rho_M M(t)\Big].
\end{aligned}
\tag{22}
$$

Combining the above system and rewrite it shortly we can have:

$$
f_i^{(j)}\equiv f_i\big(X_1(j),X_2(j),X_3(j),X_4(j),u_1(j),u_2(j)\big)\ \ (i=1,2,3,4).
$$

The superscript $^{(j)}$ represent the value of each functions at $j-th$ time point.

In similar manner corresponding to the adjoint variables $\theta_i(i=1,2,3,4)$ let us construct the functions $g_i(i=1,2,3,4)$ as following:

$$
\begin{aligned}
g_1(t) &= \mathcal{L}^{(a-1)}\Big[-\theta_1\Big[\mu\Big(1-\frac{2T}{T^{\max}}\Big)-\frac{\gamma_1(1-u_1)D}{1+\delta_1 M}-\eta K\\
&\quad -\rho_T\Big]+\theta_2\Big[\frac{\gamma_2(1-u_2)D}{1+\delta_2 M}\Big]-\theta_3\Big[\frac{\gamma_1(1-u_1)D}{1+\delta_1 M}\\
&\quad +\frac{\gamma_2(1-u_2)D}{1+\delta_2 M}\Big]\Big],\\
g_2(t) &= \mathcal{L}^{(a-1)}\Big[\theta_1\Big[\frac{\gamma_1(1-u_1)T}{1+\delta_1 M}\Big]+\theta_2\Big[\frac{\gamma_2(1-u_2)T}{1+\delta_2 M}+\rho_D\Big]\\
&\quad -\theta_3\Big[\frac{\gamma_1(1-u_1)T}{1+\delta_1 M}+\frac{\gamma_2(1-u_2)T}{1+\delta_2 M}\Big]\Big],\\
g_3(t) &= \mathcal{L}^{(a-1)}\Big[-2K+\theta_1\big[\eta T\big]+\theta_3\big[\rho_K\big]\Big],\\
g_4(t) &= \mathcal{L}^{(a-1)}\Big[-\theta_1\Big[\frac{\delta_1\gamma_1(1-u_1)TD}{(1+\delta_1 M)^2}\Big]\\
&\quad -\theta_2\Big[\frac{\delta_2\gamma_2(1-u_2)TD}{(1+\delta_2 M)^2}\Big]+\theta_3\Big[\frac{\delta_1\gamma_1(1-u_1)TD}{(1+\delta_1 M)^2}\\
&\quad +\frac{\delta_2\gamma_2(1-u_2)TD}{(1+\delta_2 M)^2}\Big]+\theta_4\Big[\rho_M\Big]\Big].
\end{aligned}
\tag{23}
$$

Combining the above system and rewrite it shortly we can have:

$$
g_i^{(j)}\equiv g_i\big(X_1(j),X_2(j),X_3(j),X_4(j),\theta_1(j),\ \theta_2(j),\theta_3(j),\theta_4(j),u_1(j),u_2(j)\big), \qquad (i=1,2,3,4).
$$

The superscript $^{(j)}$ represent the value of each functions at $j-th$ time point.

In the beginning, we explain a numerical approach using the Forward-Backward Sweep Method (FBSM) by the following steps:

- Step 1. (Initialization)

  1. a: Order of the fractional derivative.
  2. Dividing the time interval $[0, t_f]$ into the n number of time steps, where $h = \frac{t_f}{n}(t_k = kh,\ k = 0, 1, \cdots, n)$ is the step size.
  3. Initial condition for each state variable $X_i(i = 1, 2, 3, 4)$ and the terminal condition for each adjoint variable $\theta_i(n)(i = 1, 2, 3, 4)$ together with the consideration of the control parameters $u_1(0)$ and $u_2(0)$.
- Step 2. (Forward Sweep for State Variables with Control)

$$X_i(t) = \text{Forward update}\big(X_i, f_i, u_i\big)\ \ \big[t = 1, 2, \cdots n-1\big].$$

- Step 3. (Backward Sweep for Adjoint Variables)

$$\theta_i(n-t) = \text{Backward update}\big(X_i, \theta_i, g_i, u_i\big),$$

where $t = 1, 2, \cdots n-1$.

- Step 4. (Update the Control Parameters)
  Updating both $u_i\ (i = 1, 2)$ by using a convex combination of the previous controls and the values given by the eq. (17) by:

$$\begin{aligned} u_1^{New}(t) &= \pi\Big[\max\Big\{0, \min\Big(1, \frac{(\theta_3-\theta_1)(\gamma_1 TD)}{2\mathcal{P}_1(1+\delta_1 M)}\Big)\Big\}\Big] \\ &\quad + (1-\pi)u_1^{Old}(t), \\ u_2^{New}(t) &= \pi\Big[\max\Big\{0, \min\Big(1, \frac{(\theta_3-\theta_2)(\gamma_2 TD)}{2\mathcal{P}_2(1+\delta_2 M)}\Big)\Big\}\Big] \\ &\quad + (1-\pi)u_2^{Old}(t). \end{aligned} \tag{24}$$

- Step 5. (Check Convergence)
  If two successive iteration provides sufficiently close values of the control parameters, then the iteration stops, otherwise repeat Step 2 to Step 5.

The Forward-Backward update rules for the control problem, formulated using the Caputo operators [(i)-(ii)], the Caputo-Fabrizio operators [(iii)-(iv)], and the Atangana-Baleanu operators [(v)-(vi)] in the Caputo sense, are presented as follows:

(i) Forward Caputo Numerical Scheme

$$\begin{aligned} X_i(1) &= X_i(0) + \frac{h^\lambda}{\Gamma(\lambda+2)}\Big[(t+1)^\lambda(t+2+\lambda) - t^\lambda(t \\ &\quad + 2 + 2\lambda)\Big] f_i^{(0)}, \\ X_i(t+1) &= X_i(0) + \frac{h^\lambda}{\Gamma(\lambda+2)}\sum_{j=1}^{t}\Big[{}^C\Xi_1 f_i^{(j)} - {}^C\Xi_2 f_i^{(j-1)}\Big], \end{aligned}$$

where $i = 1, 2, 3, 4$ and $t = 1, 2, \cdots, n-1$.

(ii) Backward Caputo Numerical Scheme

$$\begin{aligned} \theta_i(n-1) &= \frac{h^\lambda}{\Gamma(\lambda+1)}\Big[(t+1)^\lambda(t+2+\lambda) - t^\lambda(t+2+2\lambda)\Big], \\ \theta_i(n-t) &= \frac{h^\lambda}{\Gamma(\lambda+1)}\sum_{j=1}^{t-1}\Big[{}^C\Xi_1 g_i^{(n-j)} - {}^C\Xi_2 g_i^{(n-j+1)}\Big], \end{aligned}$$

where $i = 1, 2, 3, 4$ and $t = 2, 3, \cdots, n$.
Here we have taken the Caputo fractional order $a = \lambda$ and the coefficients ${}^C\Xi_i (i = 1, 2)$ are given by:

$$\begin{aligned} {}^C\Xi_1 &= (t-j+1)^\lambda(t-j+2+\lambda) - (t-j)^\lambda(t-j+2 \\ &\quad + 2\lambda), \\ {}^C\Xi_2 &= (t-j+1)^{(\lambda+1)}(t-j+2+\lambda) - (t-j)^\lambda(t-j \\ &\quad + 1 + \lambda). \end{aligned}$$

(iii) Forward Caputo-Fabrizio Numerical Scheme

$$\begin{aligned} X_i(1) &= X_i(0) + \Big[\frac{1}{2}(2-\zeta)(1-\zeta) + \frac{3h}{4}\zeta(2-\zeta)\Big] f_i^{(0)}, \\ X_i(t+1) &= X_i(t) + \Big[{}^{CF}\Xi_1 f_i^{(t)} - {}^{CF}\Xi_2 f_i^{(t-1)}\Big], \end{aligned}$$

where $i = 1, 2, 3, 4$ and $t = 1, 2, \cdots, n-1$.

(iv) Backward Caputo-Fabrizio Numerical Scheme

$$\begin{aligned} \theta_i(n-1) &= \Big[\frac{1}{2}(2-\zeta)(1-\zeta) + \frac{3h}{4}\zeta(2-\zeta)\Big] g_i^{(n)}, \\ \theta_i(n-t) &= \theta_i(n-t+1) + \Big[{}^{CF}\Xi_1 g_i^{(n-t+1)} \\ &\quad - {}^{CF}\Xi_2 g_i^{(n-t+2)}\Big], \end{aligned}$$

where $i = 1, 2, 3, 4$ and $t = 1, 2, \cdots, n-1$.
We have taken the Caputo-Fabrizio fractional order $a = \zeta$ and the coefficients ${}^{CF}\Xi_i (i = 1, 2)$ are given by:

$$\begin{aligned} {}^{CF}\Xi_1 &= \frac{1}{2}(2-\zeta)(1-\zeta) + \frac{3h}{4}\zeta(2-\zeta), \\ {}^{CF}\Xi_2 &= \frac{1}{2}(2-\zeta)(1-\zeta) + \frac{h}{4}\zeta(2-\zeta). \end{aligned}$$

(v) Forward Atangana-Baleanu Numerical Scheme

$$\begin{aligned} X_i(1) &= X_i(0) + {}^{ABC}\Xi_1 f_i^{(0)} + {}^{ABC}\Xi_2\Big[(t+1)^\alpha(t+2 \\ &\quad + \alpha) - t^\alpha(t+2+2\alpha)\Big] f_i^{(0)}, \\ X_i(t+1) &= X_i(0) + {}^{ABC}\Xi_1 f_i^{(t)} + {}^{ABC}\Xi_2 \sum_{j=1}^{t}\Big[{}^C\Xi_1^{(\alpha)} f_i^{(j)} \\ &\quad - {}^C\Xi_2^{(\alpha)} f_i^{(j-1)}\Big], \end{aligned}$$

where $i = 1, 2, 3, 4$ and $t = 1, 2, \cdots, n-1$.

(vi) Backward Atangana-Baleanu Numerical Scheme

$$\begin{aligned} \theta_i(n-1) &= {}^{ABC}\Xi_1 g_i^{(n)} + {}^{ABC}\Xi_2\Big[(t+1)^\alpha(t+2+\alpha) \\ &\quad - t^\alpha(t+2+2\alpha)\Big] g_i^{(n)}, \\ \theta_i(n-t) &= {}^{ABC}\Xi_1 g_i^{(n-t+1)} + {}^{ABC}\Xi_2 \sum_{j=1}^{t-1}\Big[{}^C\Xi_1^{(\alpha)} g_i^{(n-j)} \\ &\quad - {}^C\Xi_2^{(\alpha)} g_i^{(n-j+1)}\Big], \end{aligned}$$

where $i = 1, 2, 3, 4$ and $t = 2, \cdots, n$.
Here, $a = \alpha$ is taken as the Atangana-Baleanu-Caputo fractional order and the coefficients are given by:

$${}^{ABC}\Xi_1 = \frac{(1-\alpha)\Gamma(\alpha)}{(1-\alpha)\Gamma(\alpha) + \alpha},$$

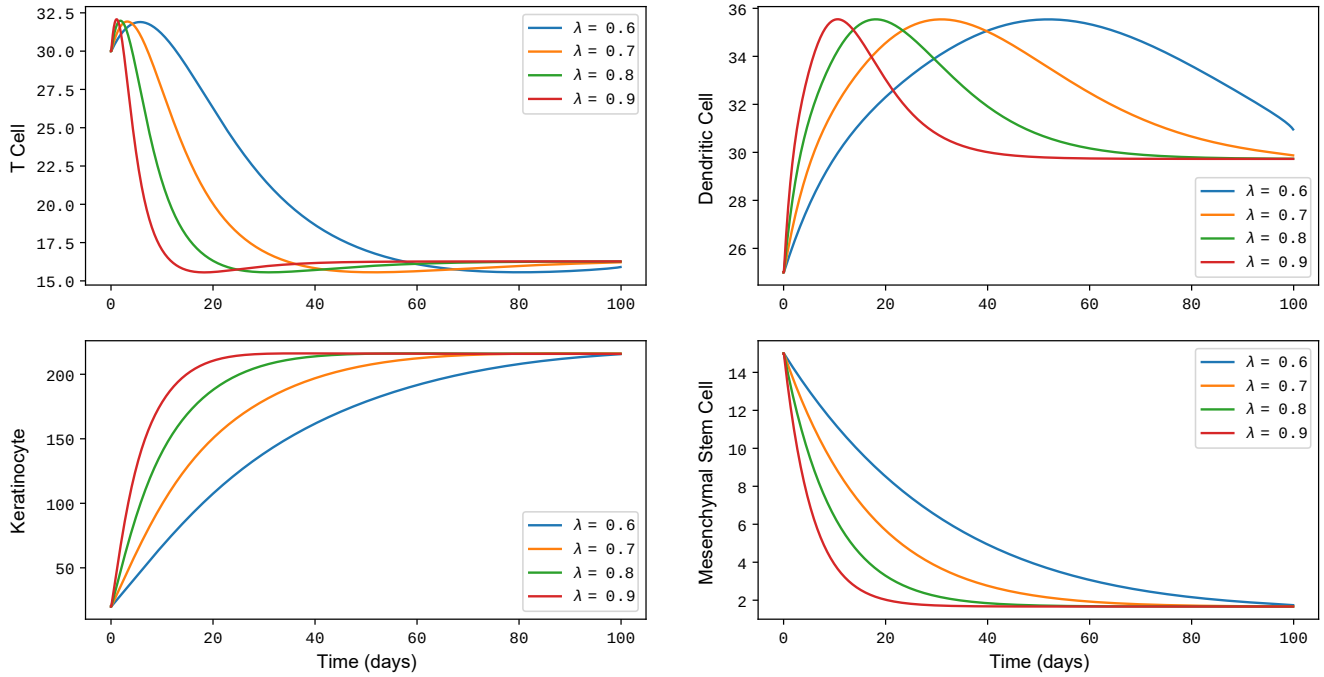

Figure 2. Population density of T cells, dendritic cells, keratinocytes, and MSCs with respect to time for different values of the fractional order λ ($= 0.6, 0.7, 0.8, 0.9$) in the Caputo sense. For this simulation, we considered the model (1) by taking the memory rate parameter value $\mathcal{L} = 0.7$.

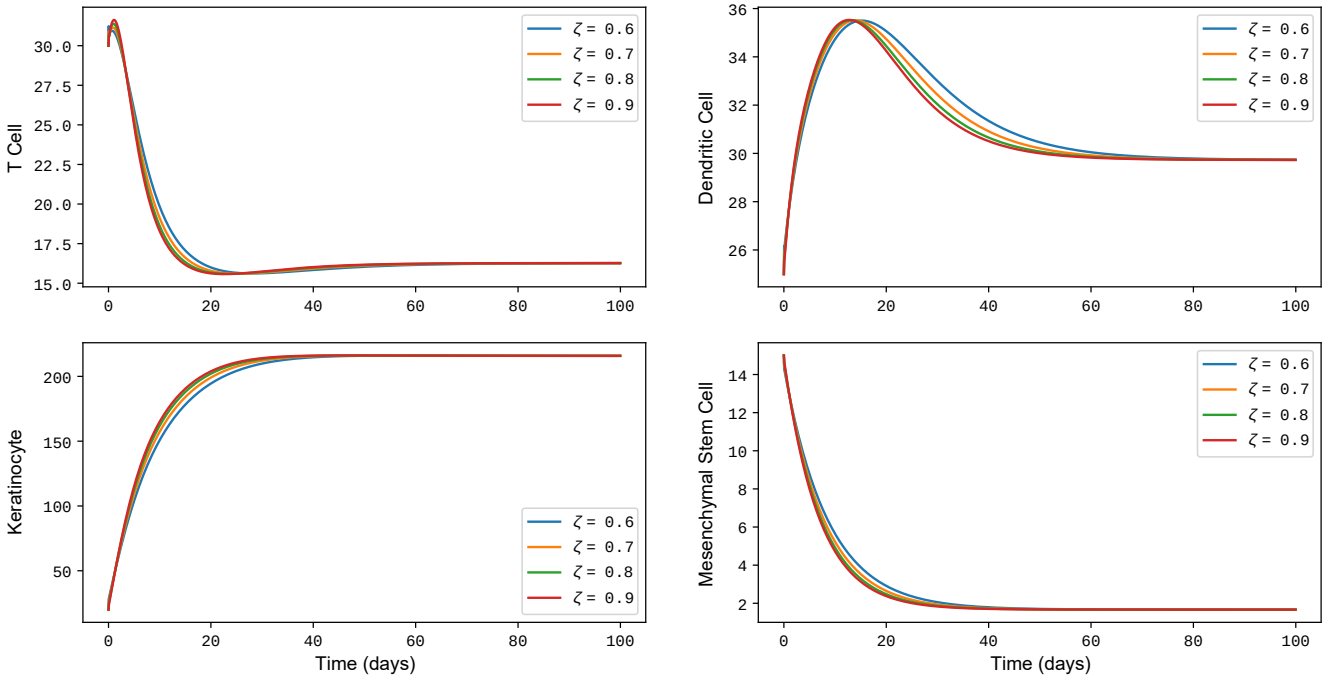

Figure 3. Population density of T cells, dendritic cells, keratinocytes, and MSCs with respect to time for different values of the fractional order ζ ($= 0.6, 0.7, 0.8, 0.9$) in the Caputo-Fabrizio sense. For this simulation, we take the memory rate parameter value $\mathcal{L} = 0.7$ by considering the model (2).

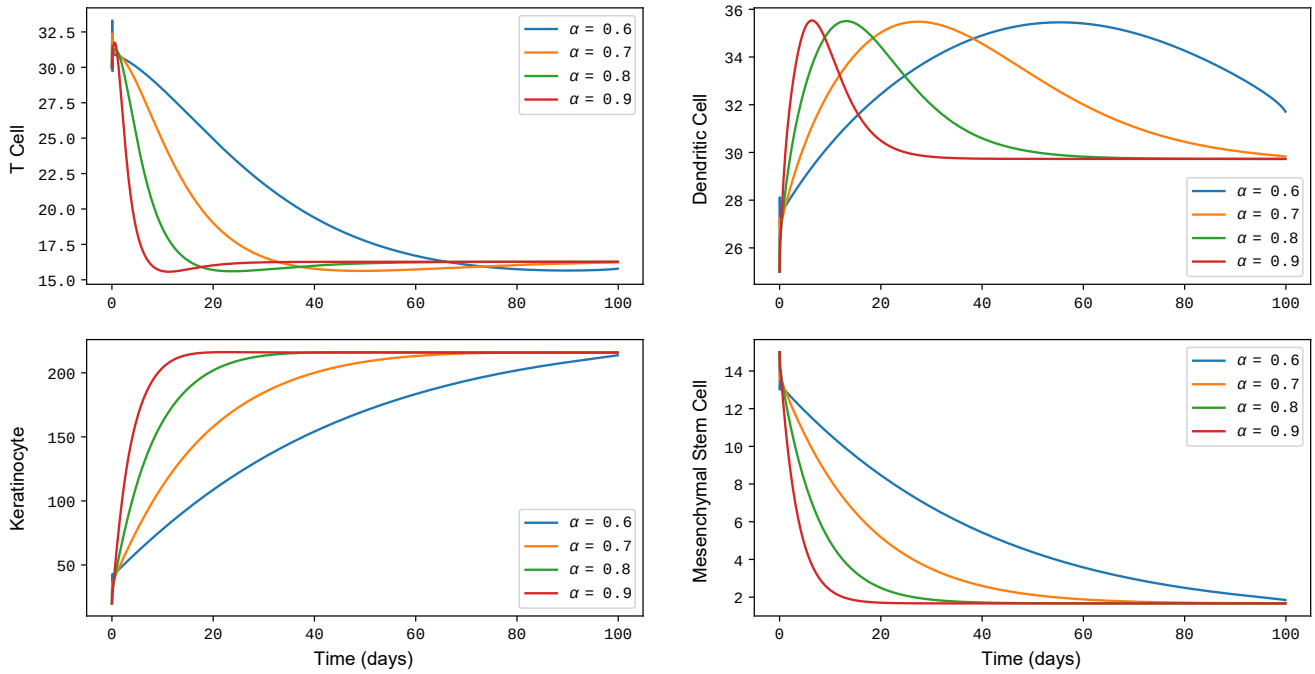

Figure 4. Population density of T cells, dendritic cells, keratinocytes, and MSCs with respect to time for different values of the fractional order α (= 0.6, 0.7, 0.8, 0.9) in the Atangana-Baleanu-Caputo sense. For this simulation, we considered the model (3) considering the memory rate parameter value $\mathcal{L} = 0.7$.

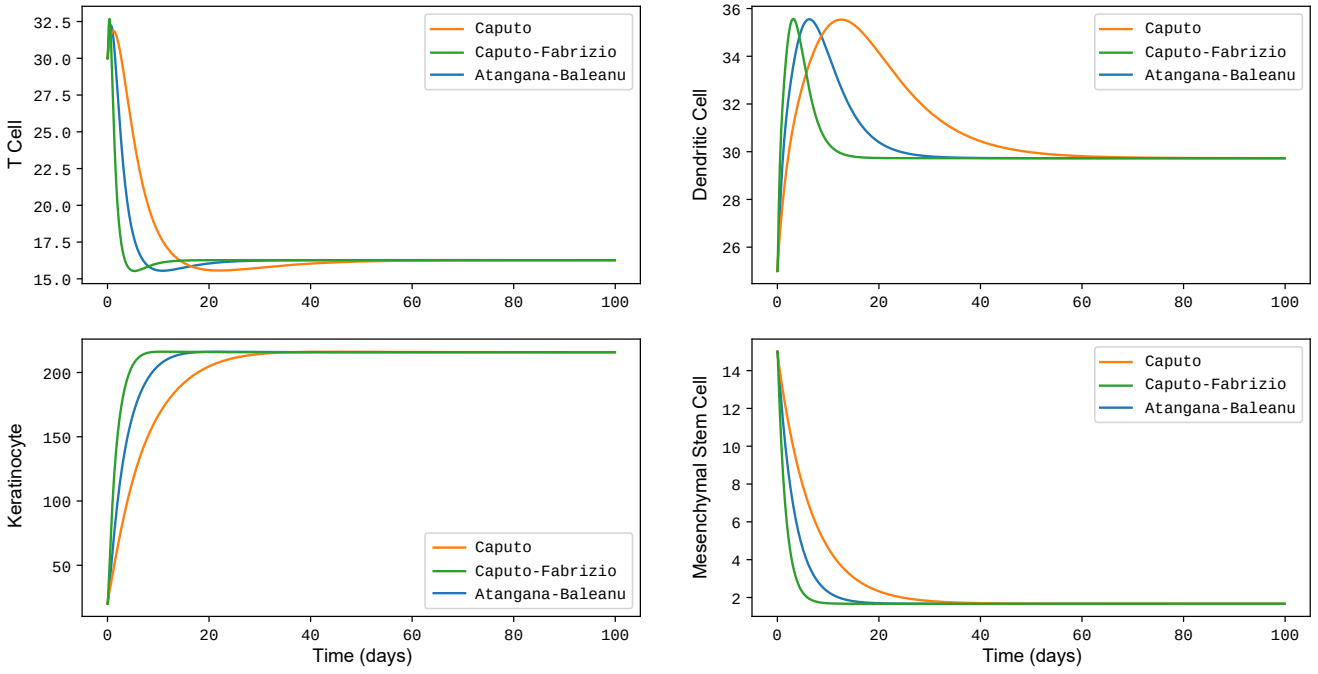

Figure 5. Time evolution of the population densities of T cells, dendritic cells, keratinocytes, and mesenchymal stem cells shown in a single plot for the models (1) to (3). The simulations are performed by fixing the memory rate parameter value of $\mathcal{L} = 0.7$, with all fractional-order parameters set to $\lambda = \zeta = \alpha = 0.9$. The dynamics are evaluated using three distinct fractional differential operators: Caputo, Caputo-Fabrizio, and Atangana–Baleanu in the Caputo sense, each with their respective kernel functions.

$$
\begin{aligned}
{}^{C}\Xi_1^{(\alpha)} &= (t-j+1)^{\alpha}(t-j+2+\alpha) - (t-j)^{\alpha}(t-j \\
&\quad +2+2\alpha), \\
{}^{ABC}\Xi_2 &= \frac{h^{\alpha}}{(\alpha+1)(1-\alpha)\Gamma(\alpha)+\alpha}, \\
{}^{C}\Xi_2^{(\alpha)} &= (t-j+1)^{(\alpha+1)}(t-j+2+\alpha) - (t-j)^{\alpha}(t \\
&\quad -j+1+\alpha).
\end{aligned}
$$

9. Numerical Simulation

In this section, we present the results of numerical simulations designed to analyze the formulated model in accordance with analytical predictions. These simulations were carefully structured to ensure consistency with fundamental mathematical principles derived from prior analytical investigations. The initial values for the model variables were selected to adhere to these foundational criteria, ensuring that the system behaves in a manner consistent with expected theoretical outcomes. To conduct these simulations, we utilized Python. The initial population values used in the simulations are set as follows: $T_0 = 30$, $D_0 = 25$, $K_0 = 20$, and $M_0 = 15$. The corresponding parameter values employed throughout the numerical experiments are listed in Table 1, providing a clear reference for the simulation setup. By employing different fractional-order derivatives, we examined how varying memory effects influence the stability and dynamics of the cell populations within the system.

The first set of simulations, depicted in Figure 2, showcases the temporal evolution of T cells, dendritic cells, keratinocytes, and mesenchymal stem cells within model (1), using the Caputo kernel function. These simulations were conducted for different values of the fractional-order parameter λ, specifically $\lambda = 0.6$, 0.7, 0.8, and 0.9. The results reveal a distinct pattern: as the value of λ decreases, the stabilization of the cell populations occurs more gradually, indicating that lower values of λ introduce a stronger memory effect. This suggests that the system retains past states for longer durations when λ is smaller, leading to delayed convergence to equilibrium. In contrast, higher values of λ result in faster stabilization, signifying that the system is less influenced by its history. This behavior highlights the significant role that fractional-order derivatives play in modeling biological processes with memory-dependent dynamics.

The second set of simulations, illustrated in Figure 3, investigates the behavior of the model under model (2) using the Caputo-Fabrizio kernel function. Here, we varied the fractional-order parameter ζ across values $\zeta = 0.6$, 0.7, 0.8, and 0.9 to assess how different fractional orders impact system stability. Unlike the Caputo kernel function, which showed a pronounced effect of ζ on stabilization rates, the Caputo-Fabrizio formulation exhibits a more uniform response across different values of ζ. This implies that the influence of fractional-order variation is less significant in this case, leading to a more consistent stabilization pattern regardless of the specific ζ value used. This observation underscores a fundamental difference between the two kernel functions: while the Caputo kernel function results in gradual stabilization for lower orders, the Caputo-Fabrizio approach produces less sensitivity to fractional-order changes, suggesting that it represents memory effects in a different manner.

The final set of simulations, represented in Figure 4, examines model (3) while varying the fractional-order parameter α ($\alpha = 0.6$, 0.7, 0.8, and 0.9), again using the Caputo kernel function. The results demonstrate a trend similar to that observed in Figure 2: as the value of α decreases, the system takes longer to reach a stable state. This reinforces the finding that lower fractional orders amplify memory effects, delaying stabilization across multiple configurations of the model. Taken together, these simulations emphasize the profound impact of fractional-order parameters on biological system behavior. The comparison between the Caputo and Caputo-Fabrizio kernel functions highlights the importance of selecting an appropriate mathematical framework when modeling dynamic systems influenced by historical dependencies. Ultimately, these insights contribute to a deeper understanding of fractional-order modeling in biological processes, offering a powerful approach for capturing the complex, memory-driven dynamics of cellular populations.

In Figure 5, we analyze the temporal evolution of the model's population densities: T cells, dendritic cells, keratinocytes, and mesenchymal stem cells, by employing three distinct numerical schemes based on the Caputo, Caputo-Fabrizio, and Atangana-Baleanu-Caputo operators. The fractional-order parameters were fixed at $\lambda = \zeta = \alpha = 0.9$ to provide a uniform basis for comparison. The results reveal a clear distinction in how each operator influences the system's stabilization behavior. Among the three approaches, the Caputo-Fabrizio operator exhibits the most rapid convergence to the stability orbit, indicating a weaker memory effect and faster adaptation of population densities to equilibrium. The Atangana-Baleanu-Caputo operator follows, displaying a moderate speed of convergence to stabilization behavior, while the Caputo operator demonstrates the slowest approach to stability, reflecting its stronger historical dependency. This finding underscores the fundamental differences in how these fractional operators encode memory effects in biological systems. The Atangana-Baleanu-Caputo scheme, by allowing for a more balanced and responsive adaptation, could be particularly useful in applications where rapid recovery and stabilization of biological populations are crucial.

In Figures 6 to 8, we extend our analysis by investigating the influence of the memory rate parameter ($\mathcal{L}$) on system dynamics while utilizing three different fractional operators: Caputo, Caputo-Fabrizio, and Atangana-Baleanu-Caputo. The fractional-order parameter was consistently set at 0.9, while $\mathcal{L}$ was varied across 0.1, 0.3, 0.5, 0.7, and 0.9. The objective was to determine whether the rate at which past states influence present behavior significantly alters population trajectories. Interestingly, the results across all three figures demonstrate minimal variation in system trajectories despite changes in $\mathcal{L}$, suggesting that within this specific modeling framework, the system exhibits low sensitivity to variations in the memory rate parameter. This indicates that while the choice of fractional operator plays a crucial role in defining system behavior, adjustments to $\mathcal{L}$ do not significantly impact the model's predictive power in this context. These insights are valuable in biological modeling, as they suggest that certain fractional-order parameters may have a dominant effect on system behavior, while others, such as the memory rate parameter $\mathcal{L}$, may have a more limited role.

We now analyze the impact of control strategies on the fractionalized model (14) under different fractional operators, applying distinct formulations across the three considered frac-

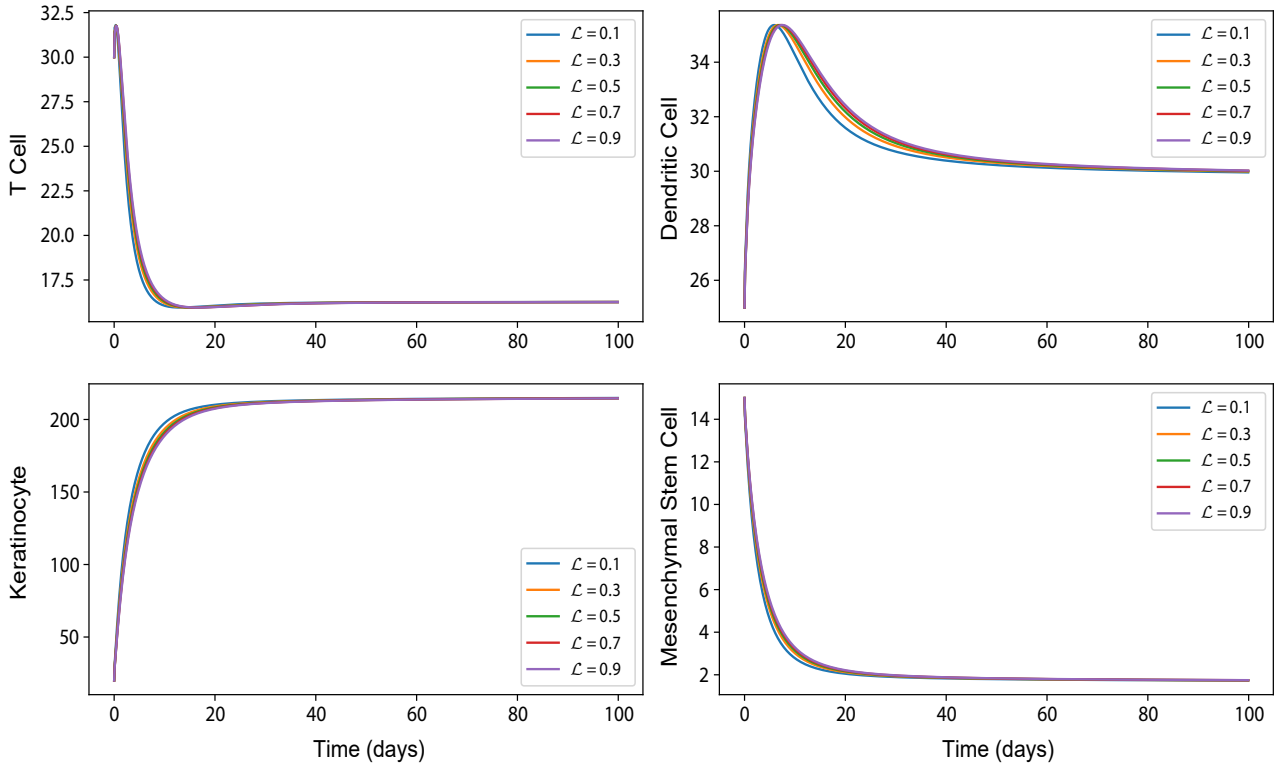

Figure 6. Temporal evolution of system population dynamics under varying memory rate parameter $\mathcal{L}$ within the Caputo fractional operator framework. The fractional order parameter is fixed at $\lambda = 0.9$, with $\mathcal{L}$ values set to 0.1, 0.3, 0.5, 0.7, and 0.9. The figure shows that the trajectories remain nearly similar despite variations in the memory rate parameter.

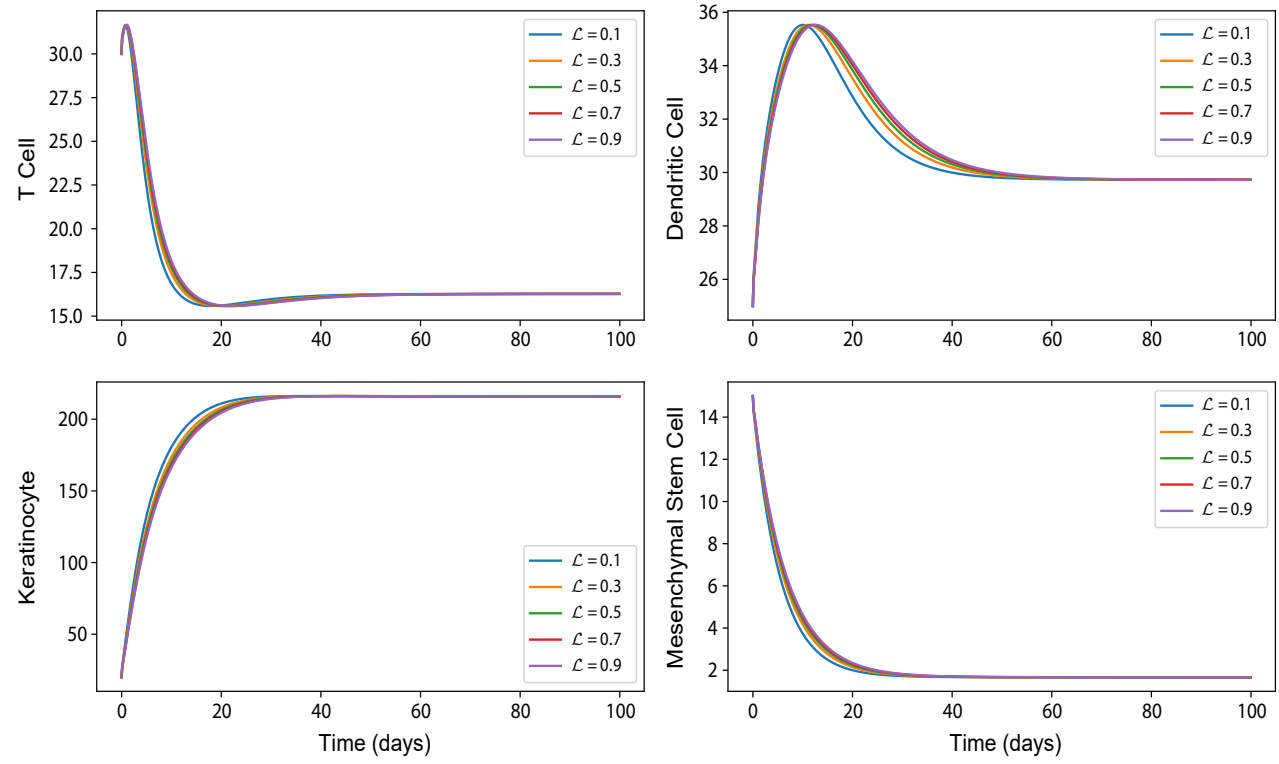

Figure 7. All system population dynamics with respect to time by varying the memory rate parameter $\mathcal{L}$ values considering the Caputo-Fabrizio fractional operator structure. The fractional order parameter is fixed at $\zeta = 0.9$, with $\mathcal{L}$ values set to 0.1, 0.3, 0.5, 0.7, and 0.9. The figure indicates that the trajectories exhibit minimal variation despite changes in the memory rate parameter.

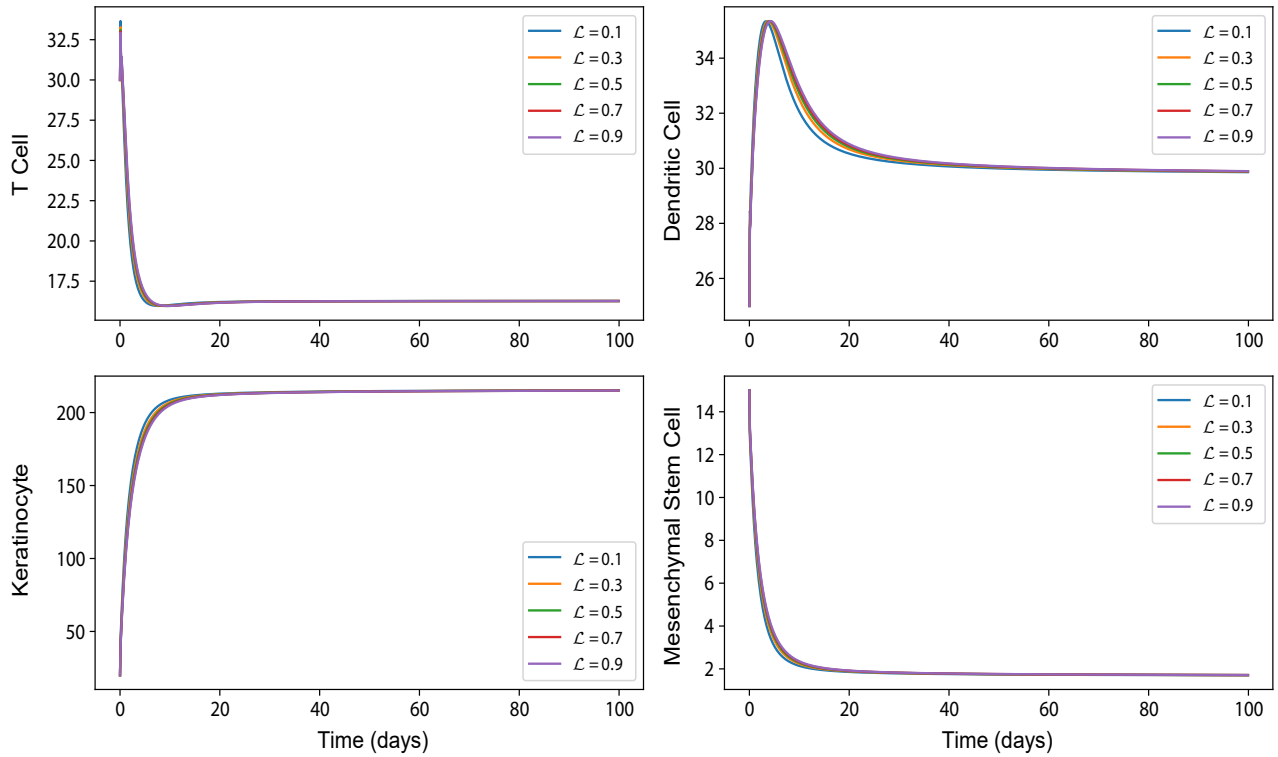

Figure 8. Using the Atangana-Baleanu-Caputo fractional scheme, all system population densities with respect to time are plotted by varying the memory rate parameter $\mathcal{L}$ values of 0.1, 0.3, 0.5, 0.7, and 0.9 while fixing the value of the fractional order parameter α at 0.9. Although the memory rate parameter changes, the figure shows that the trajectories show negligible variation.

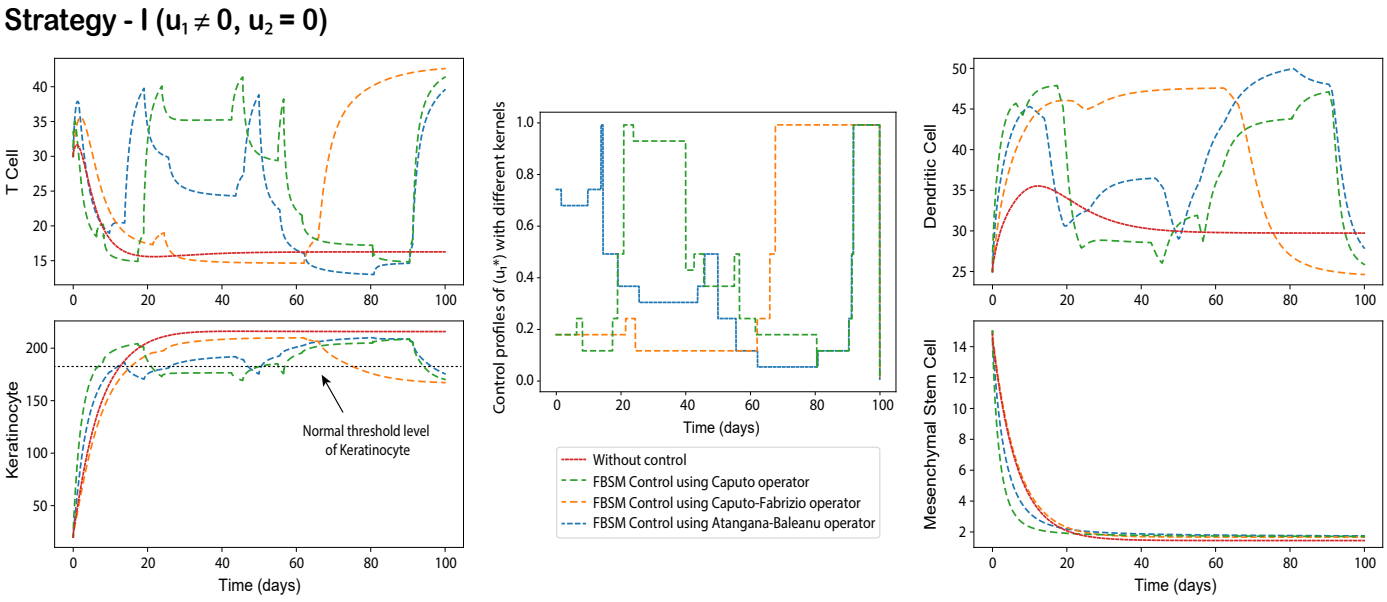

Figure 9. Control-induced system along with the control profile of the optimal control functions, considering $u_1 \neq 0, u_2 = 0$, over time using three different fractional operator kernels: Caputo, Caputo-Fabrizio, and Atangana-Baleanu. The uncontrolled system populations are represented by red solid trajectories, while the fractional-order controlled systems are illustrated using different colored dotted trajectories corresponding to the respective kernels. The control functions highlight how each kernel's distinct memory effect influences the density and timing of optimal treatment interventions required to regulate the immune response.

tional approaches. This step aims to enhance our understanding of how various mathematical interpretations of fractional dynamics can be utilized to design effective control interventions relevant to real-world scenarios. For the numerical implementation of optimal control strategies via the Forward-Backward Sweep Method (FBSM), all fractional orders are fixed as $\lambda = \zeta = \alpha = 0.9$, and the memory rate parameter is set to $\mathcal{L} = 0.7$. The weight constants in the objective functional are chosen as $\mathcal{P}_1 = \mathcal{P}_2 = 0.5$, and all other parameter values used in the simulations are taken from Table 1.

- Strategy-I ($u_1 \neq 0, u_2 = 0$)
  In this control strategy, we investigate the effects of administering a TNF-α inhibitor by setting $u_1 \neq 0$, while excluding the use of an IL-23 blocker by fixing $u_2 = 0$. Figure 9, provides a comparative analysis between the uncontrolled system (depicted by red trajectories) and the controlled system, which is simulated using three different fractional operators: Caputo, Caputo-Fabrizio, and Atangana-Baleanu-Caputo—through FBSM. The controlled system is represented using three distinct colored dotted trajectories, corresponding to each fractional operator, allowing for a direct comparison of their effects on population dynamics. Additionally, the control profile of u_1 is illustrated to capture its evolution under the influence of the three kernel functions. The numerical results in Figure 9, reveal that TNF-α inhibition leads to a gradual, but not substantial, decline in keratinocyte density, indicating partial suppression of the inflammatory response. T cell density increases significantly, while dendritic cell density decreases. These outcomes suggest that while TNF-α inhibition can diminish certain pro-inflammatory pathways, it does not fully eliminate immune activation, resulting in a partial disruption of cytokine-mediated interactions but not complete normalization of keratinocyte proliferation. The different responses observed across the three fractional operators highlight the importance of memory effects, as each approach captures unique aspects of immune regulation and inflammation dynamics.
- Strategy-II ($u_1 = 0, u_2 \neq 0$)
  In this control strategy, we focus on the effects of an IL-23 blocker by setting $u_2 \neq 0$, while excluding the use of a TNF-α inhibitor by fixing $u_1 = 0$. Again in Figure 10, we compare controlled and uncontrolled dynamics across the same three fractional operators (distinguished by different colored trajectories). The control profile of u_2 is illustrated. Simulations show a slight reduction in keratinocyte density, though levels remain above healthy thresholds, indicating that IL-23 blockade alone is insufficient to achieve complete disease remission. Additionally, T-cell density declines modestly, whereas dendritic cell density increases, pointing to limited regulation of the immune response. Biologically, these results imply that IL-23 inhibition alone cannot fully disrupt the inflammatory cytokine network, allowing immune infiltration to persist and thus preventing restoration of tissue homeostasis. Note that, across all three fractional operators, similar population trends are observed, suggesting that under the control of IL-23 inhibition, the memory effects inherent to each operator do not significantly alter the qualitative behavior of the system. This emphasizes the potential need for a combined therapeutic approach.
- Strategy-III ($u_1 \neq 0, u_2 \neq 0$)
  In this control strategy, we conduct numerical simulations on fractionalized systems represented by models (1) to (3), governed by three distinct fractional-order differential operators: Caputo, Caputo-Fabrizio, and Atangana-Baleanu-Caputo, to evaluate the behavior of the model under simultaneous application of both control measures: the TNF-α inhibitor ($u_1 \neq 0$) and IL-23 blocker ($u_2 \neq 0$) (see Figure 11). The red trajectories depict the uncontrolled system, while the controlled responses are illustrated by three differently colored dotted trajectories corresponding to each fractional operator, allowing a comparative assessment of the system's dynamics. The evolution of the control profiles u_1 and u_2 are also presented, reflecting how each fractional kernel influences treatment intensity over time. Results indicate that the combined control strategy successfully reduces keratinocyte density to a healthy state, effectively curing inflammation-induced proliferation. The densities of T cells and dendritic cells increase significantly. Biologically, this implies that cytokine-driven inflammatory interactions are suppressed, slowing immune infiltration, a key contributor to psoriasis progression. Notably, the Caputo and Atangana-Baleanu-Caputo operators exhibit similar trends across all cell populations, indicating comparable memory effects, whereas the Caputo-Fabrizio operator produces distinct control profiles and immune dynamics due to its faster memory decay. These differences underscore that for a fixed fractional-order parameter value, optimal control strategies depend on the chosen operator: Caputo demands sustained interventions due to strong memory retention, suitable for chronic cases; Caputo-Fabrizio allows short-term interventions, making it ideal for acute flares but less effective for long-term control; and Atangana-Baleanu-Caputo offers a balanced memory effect, supporting a hybrid approach with intensive early therapy followed by maintenance dosing. These findings emphasize the importance of fractional-order modelling in tailoring control strategies, as varying memory effects directly influence the design and efficacy of therapeutic interventions.

Figure 12 presents the effectiveness analysis (in %) of three control strategies using bar plots, with fixed fractional parameters $\lambda = \zeta = \alpha = 0.9$. From a biological perspective, Strategy I (e.g., targeting a single pathway) shows moderate effectiveness, with the Caputo–Fabrizio operator yielding the best outcome. Strategy II (targeting an alternative pathway) shows weaker responses with comparable results across all operators, where the Caputo operator performs slightly better. Strategy III, representing a combined therapeutic approach (e.g., TNF-α and IL-23 inhibition), demonstrates the highest effectiveness, particularly under the Caputo–Fabrizio operator. These results suggest that combination therapy provides superior control over psoriatic inflammation.

Additionally, Figure 13 presents a global sensitivity analysis of key model parameters affecting the keratinocyte population, using Latin Hypercube Sampling (LHS) combined with the Partial Rank Correlation Coefficients (PRCC) method. For each parame-

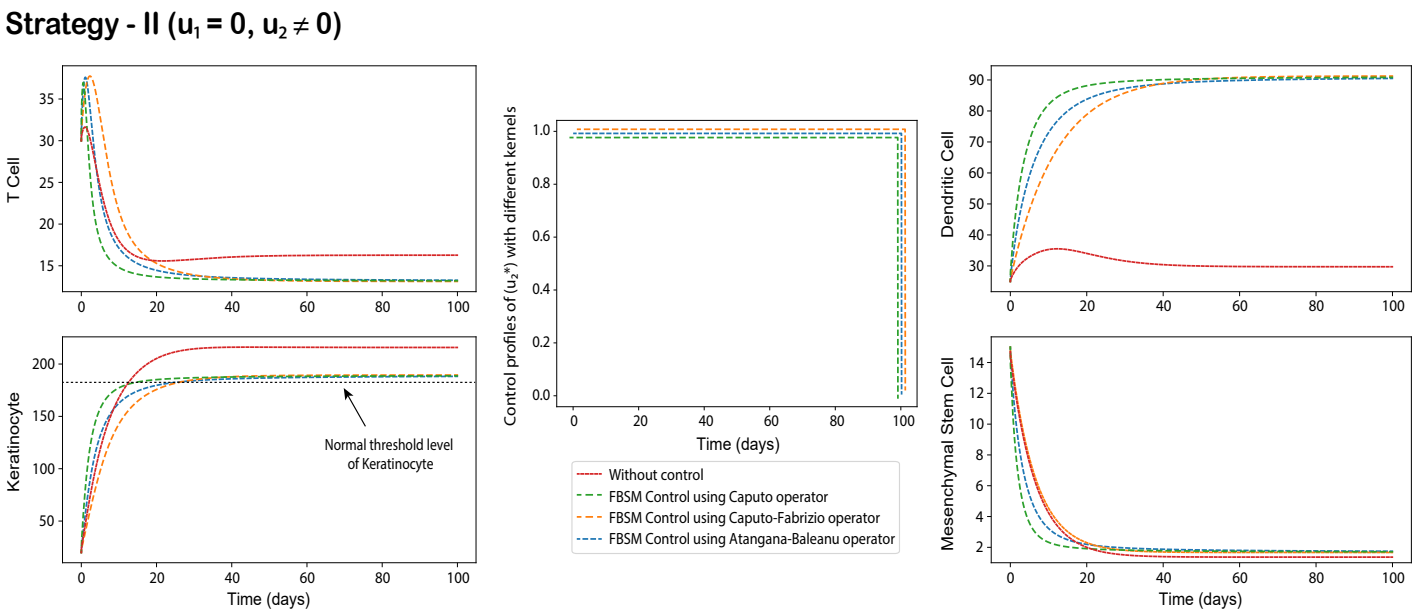

Figure 10. Comparison of the uncontrolled and controlled system dynamics under the influence of the optimal control function $u_2 \neq 0$ while $u_1 = 0$, utilizing three fractional operator kernels: Caputo, Caputo-Fabrizio, and Atangana-Baleanu. Red solid trajectories represent the uncontrolled system populations, whereas the controlled system is depicted through distinct colored dotted trajectories corresponding to each fractional operator. The control profiles illustrate the impact of different kernel memory effects on the timing and intensity of optimal treatment interventions for immune response regulation.

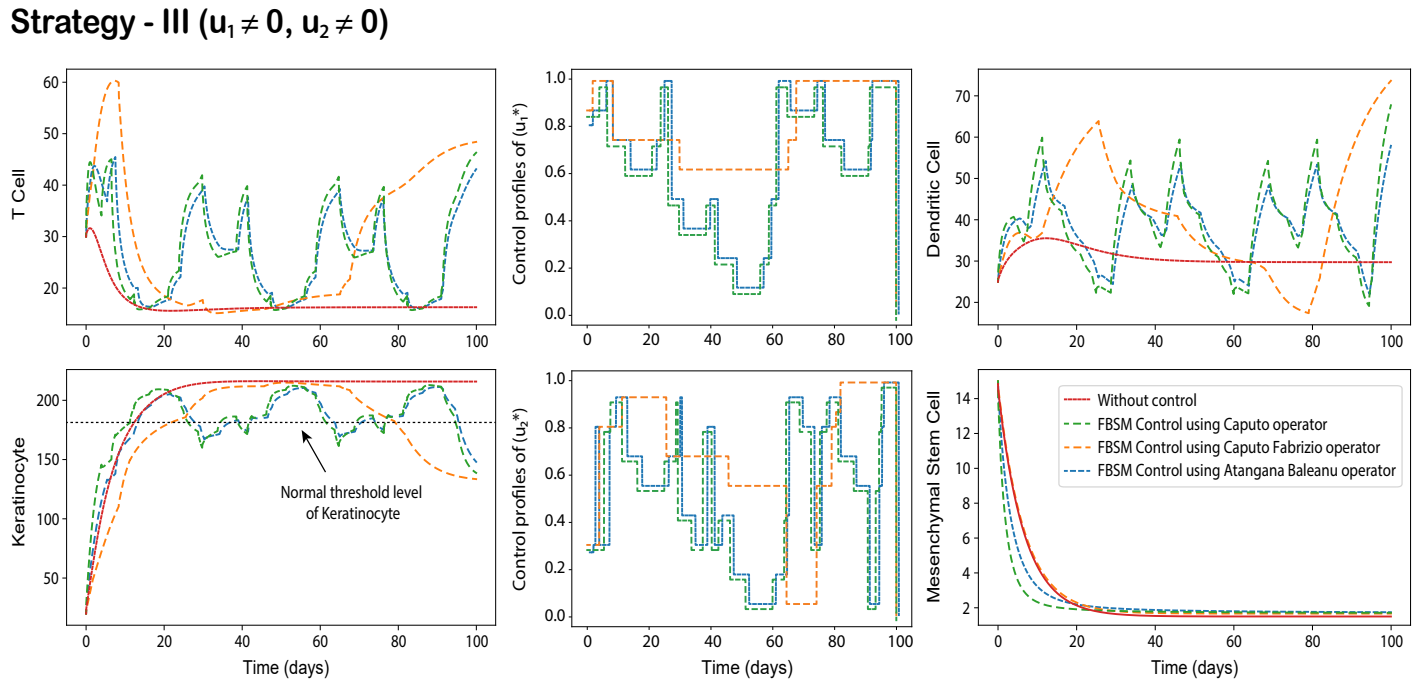

Figure 11. Visualization of the system dynamics under both control functions ($u_1 \neq 0, u_2 \neq 0$) compared to the uncontrolled case, using three fractional operator kernels: Caputo, Caputo-Fabrizio, and Atangana-Baleanu. The red solid trajectories indicate the uncontrolled system populations, while the controlled system is represented by colored dotted trajectories corresponding to each fractional operator. The control profiles demonstrate how the distinct memory effects of each kernel influence the optimal timing and magnitude of treatment interventions for immune response regulation.

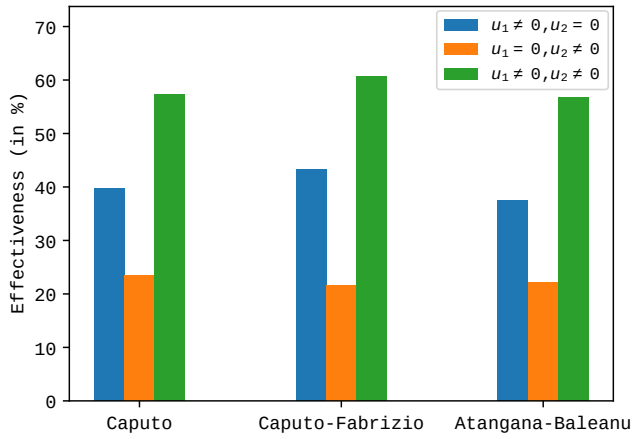

Figure 12. Effectiveness analysis of control strategies I (blue), II (orange), and III (green), expressed in percentage, for the three considered fractional operators with fixed fractional parameters $\lambda = \zeta = \alpha = 0.9$. Strategy I shows that the moderate effectiveness with all considered operators, among them Caputo–Fabrizio, yields the highest effectiveness. Strategy II demonstrates weaker effectiveness, and the control using all fractional operators provides almost similar outcomes. Among them, the Caputo operator provides the highest effectiveness. Strategy III, the combined strategy, provides the strongest overall results, with the Caputo–Fabrizio operator again achieving the highest effectiveness among all operators.

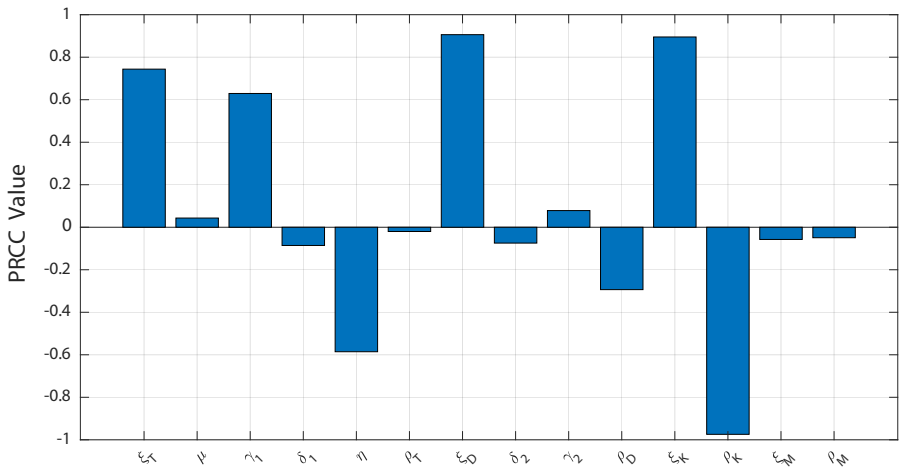

Figure 13. Partial Rank Correlation Coefficient (PRCC) bar plots of system parameters with respect to the keratinocyte population, based on a sample size of 1000. PRCC values are computed at day 100, with all p-values reported up to four decimal places. The horizontal axis represents the model parameters, while the vertical axis indicates their corresponding PRCC values.

ter, the PRCC and corresponding p-value are computed; a p-value < 0.05 indicates statistical significance. The bar plot reveals that parameters ξ_T, μ, γ_1, ξ_D, γ_2, and ξ_K positively influence disease progression, whereas δ_1, η, ρ_T, δ_2, ρ_D, ρ_K, ξ_M, and ρ_M exert negative effects. Keratinocyte levels are used as a marker for disease prediction, and the sensitivity analysis helps identify key parameters that could serve as potential targets for therapeutic intervention in psoriasis.

10. Discussion and Conclusion

Ordinary differential equations (ODEs) are commonly used to describe biological systems by modeling instantaneous processes that respond immediately to changes in time. However, they often fail to account for historical dependencies, which are crucial in biological systems influenced by cumulative past effects. In contrast, fractional differential equations (FDEs) introduce a memory effect, allowing past states of the system to influence present dynamics through fractional-order parameters. In this study, we implemented FDEs within a cell-biological model of psoriasis and analyzed its behavior under three different fractional operators: Caputo, Caputo-Fabrizio, and Atangana-Baleanu-Caputo. The results reveal that decreasing the fractional parameters λ (in the Caputo operator) and α (in the Atangana-Baleanu-Caputo operator) leads to a slower stabilization of the system, suggesting a stronger memory effect. However, in the Caputo-Fabrizio model, the population trajectories exhibit similar stabilization behavior across different values of the fractional parameter ζ, indicating that this operator represents memory effects differently. This memory-driven framework reflects how keratinocyte and mesenchymal stem cell (MSC) populations gradually reach equilibrium, particularly under the Caputo and Atangana-Baleanu-Caputo formulations. The key advantage of

using fractional-order operators lies in their non-local nature, which provides infinite degrees of freedom in selecting appropriate fractional parameters, leading to more precise and adaptable models compared to classical ODE-based approaches. Furthermore, the retention of memory effects enables these models to capture complex biological dynamics more accurately over time, overcoming the limitations of integer-order models that assume instantaneous changes without historical influence.

By integrating an optimal drug dosing strategy within the fractional-order system, we observed greater reductions in keratinocyte populations, reinforcing the effectiveness of the FDE model in capturing psoriasis dynamics compared to traditional ODE systems. To further explore the therapeutic impact of memory effects, we applied optimal control theory to assess the influence of two biologic drugs: TNF-α inhibitors and IL-23 blockers. Utilizing the Forward-Backward Sweep Method (FBSM), we numerically simulated three distinct treatment strategies under each of the three fractional operators. The simulation results demonstrate that the third strategy (Strategy III), which employs a combination of both TNF-α inhibitors and IL-23 blockers, yields the most optimal therapeutic outcome. We have confirmed this by effectiveness analysis in percentage, especially the Caputo-Fabrizio operator yielding the best outcome. Under this combined treatment approach, keratinocyte density successfully returns to a healthy state, and the inflammatory cytokine interactions and immune cell infiltration are effectively suppressed. These findings highlight the superior predictive capability of fractional-order models in designing targeted therapeutic strategies for psoriasis. The ability of fractional models to account for long-term effects and varying degrees of memory makes them particularly well-suited for understanding disease progression and optimizing long-term treatment regimens. However, this study has a few notable limitations. Firstly, the model simplifies the biological complexity by focusing on selected immune cell populations (T cells, dendritic cells, keratinocytes, and mesenchymal stem cells) while omitting the other triggering factors, such as impacts of other cell components and their abnormal differentiation and consideration of cytokines as model components. Secondly, many parameter values are assumed or adapted. A significant challenge in model validation arises, and error analysis occurs due to a lack of experimental cellular-level data. Future extensions of this work can focus on addressing the above limitations to further enhance the model's predictive and therapeutic relevance. Incorporating additional immune mediators, especially key cytokines, would offer a more complete representation of psoriatic inflammation. Spatial aspects of psoriatic inflammation could be incorporated by space-fractional or reaction-diffusion equations to better capture the localized nature of the disease. Investigating stem cell-based therapeutic control strategies within the fractional-order framework may provide more effective outcomes. Additionally, combining the model with parameter optimization techniques and data-driven fractional modeling could improve the accuracy and applicability of the system.

Author Contributions. **Kushary, S.**: Conceptualization, visualization, methodology, software, formal analysis, writing—original draft preparation, writing—review and editing. **Ghosh, T.**: Visualization, methodology, formal analysis, writing—original draft preparation. **Makinde, O. D.**: Investigation, validation, writing—review and editing. **Li, X.**: Visualization, investigation, validation, resources. **Roy, P. K.**: Conceptualization, investigation, validation, writing—review and editing, Supervision.

Acknowledgement. The authors are thankful to the editors and reviewers who have supported us to improve this manuscript.

Funding. This research work is supported by the DST FIST Programme, Government of India [No. SR/FST/MS-II/2021/101(C)], Department of Mathematics, Jadavpur University, Kolkata-700032, India. Tushar Ghosh is supported by the UGC-JRF (NTA Ref. No. 211610107883), New Delhi, India. Xue-Zhi Li is supported by the National Natural Science Foundation of China (No. 12271143).

Conflict of interest. The authors declare no conflict of interest.

Data availability. Not applicable.

References

[1] P. Łakuta *et al.*, "How does stigma affect people with psoriasis?" *Advances in Dermatology and Allergology/Postępy Dermatologii i Alergologii*, vol. 34, no. 1, pp. 36–41, 2017. DOI:10.5114/pdia.2016.62286

[2] A. Menter *et al.*, "Guidelines of care for the management of psoriasis and psoriatic arthritis: Section 1. overview of psoriasis and guidelines of care for the treatment of psoriasis with biologics," *Journal of the American Academy of Dermatology*, vol. 58, no. 5, pp. 826–850, 2008. DOI:10.1016/j.jaad.2008.02.039

[3] C. Albanesi *et al.*, "The interplay between keratinocytes and immune cells in the pathogenesis of psoriasis," *Frontiers in Immunology*, vol. 9, p. 1549, 2018. DOI:10.3389/fimmu.2018.01549

[4] P. Blanco *et al.*, "Dendritic cells and cytokines in human inflammatory and autoimmune diseases," *Cytokine & growth factor reviews*, vol. 19, no. 1, pp. 41–52, 2008. DOI:10.1016/j.cytogfr.2007.10.004

[5] Y. Deng, C. Chang, and Q. Lu, "The inflammatory response in psoriasis: a comprehensive review," *Clinical reviews in allergy & immunology*, vol. 50, no. 3, pp. 377–389, 2016. DOI:10.1007/s12016-016-8535-x

[6] Y. Zheng *et al.*, "Interleukin-22, a th17 cytokine, mediates il-23-induced dermal inflammation and acanthosis," *Nature*, vol. 445, no. 7128, pp. 648–651, 2007. DOI:10.1038/nature05505

[7] A. Datta and P. K. Roy, "T-cell proliferation on immunopathogenic mechanism of psoriasis: a control based theoretical approach," *Control and Cybernetics*, vol. 42, no. 2, pp. 365–386, 2013.

[8] I. Ullah, R. B. Subbarao, and G. J. Rho, "Human mesenchymal stem cells-current trends and future prospective," *Bioscience reports*, vol. 35, no. 2, p. e00191, 2015. DOI:10.1042/BSR20150025

[9] L. Cheng *et al.*, "Human umbilical cord mesenchymal stem cells for psoriasis: a phase 1/2a, single-arm study," *Signal Transduction and Targeted Therapy*, vol. 7, no. 1, p. 263, 2022. DOI:10.1038/s41392-022-01059-y

[10] N. J. Savill, R. Weller, and J. A. Sherratt, "Mathematical modelling of nitric oxide regulation of rete peg formation in psoriasis," *Journal of theoretical biology*, vol. 214, no. 1, pp. 1–16, 2002. DOI:10.1006/jtbi.2001.2400

[11] H. B. Oza *et al.*, "Modelling and finite-time stability analysis of psoriasis pathogenesis," *International Journal of Control*, vol. 90, no. 8, pp. 1664–1677, 2017. DOI:10.1080/00207179.2016.1217566

[12] H. Zhang *et al.*, "Modelling epidermis homoeostasis and psoriasis pathogenesis," *Journal of The Royal Society Interface*, vol. 12, no. 103, p. 20141071, 2015. DOI:10.1098/rsif.2014.1071

[13] A. K. Roy, M. Nelson, and P. K. Roy, "A control-based mathematical study on psoriasis dynamics with special emphasis on il- 21 and ifn- γ interaction network," *Mathematical Methods in the Applied Sciences*, vol. 44, no. 17, pp. 13403–13420, 2021. DOI:10.1002/mma.7635

[14] S. Kushary, P. K. Roy, and X. Cao, "Introducing msc therapy to inhibit Th_1 and TH_17 mediated cytokines: A mathematical study to regulate psoriasis," in *International Conference on Mathematical Analysis and Application in Modeling*, pp. 87–101, 2023. DOI:10.1007/978-981-97-9194-1_7

[15] A. A. Nelson *et al.*, "Cost-effectiveness of biologic treatments for psoriasis based on subjective and objective efficacy measures assessed over a 12-week treatment period," *Journal of the American Academy of Dermatology*, vol. 58, no. 1, pp. 125–135, 2008. DOI:10.1016/j.jaad.2007.09.018

[16] M. Lebwohl *et al.*, "Combination therapy to treat moderate to severe psoriasis," *Journal of the American Academy of Dermatology*, vol. 50, no. 3, pp. 416–430, 2004. DOI:10.1016/j.jaad.2002.12.002
[17] A. K. Roy, F. Al Basir, and P. K. Roy, "A vivid cytokines interaction model on psoriasis with the effect of impulse biologic (TNF-α inhibitor) therapy," *Journal of Theoretical Biology*, vol. 474, pp. 63–77, 2019. DOI:10.1016/j.jtbi.2019.04.007
[18] A. K. Roy *et al.*, "A model analysis to measure the adherence of etanercept and fezakinumab therapy for the treatment of psoriasis," *Nonlinear Analysis: Modelling and Control*, vol. 27, no. 3, pp. 1–21, 2022. DOI:10.15388/namc.2022.27.26483
[19] R. Agarwal and C. Midha, "Study and mathematical analysis of the novel fractional bone mineralization model." *Journal of Computational Analysis & Applications*, vol. 33, no. 1, 2024.
[20] R. Agarwal, P. Airan, and C. Midha, "Mathematical analysis of the nonlinear dynamics of bone mineralization," in *Mathematical Methods in Medical and Biological Sciences*, pp. 207–225, 2025. DOI:10.1016/B978-0-44-328814-2.00017-5
[21] R. R. Musafir *et al.*, "Comparison of fractional-order monkeypox model with singular and non-singular kernels," *Jambura Journal of Biomathematics (JJBM)*, vol. 5, no. 1, pp. 1–9, 2024. DOI:10.37905/jjbm.v5i1.24920
[22] K. Das *et al.*, "A qualitative analysis of leukemia fractional order sicw model," *Jambura Journal of Biomathematics (JJBM)*, vol. 5, no. 1, pp. 46–53, 2024. DOI:10.37905/jjbm.v5i1.24961
[23] A. Pandey and S. Ghosh, "Numerical study of childhood disease model with lyapunov stability analysis," *Indian Journal of Physics*, vol. 99, pp. 3393–3408, 2025. DOI:10.1007/s12648-024-03537-1
[24] S. Kushary *et al.*, "A mathematical insight to control the disease psoriasis using mesenchymal stem cell transplantation with a biologic inhibitor," *Scientific Reports*, vol. 14, no. 1, p. 21897, 2024. DOI:10.1038/s41598-024-71251-3
[25] M. Caputo, *Elasticit'a e dissipazione*. Zanichelli, 1965.
[26] M. Caputo and M. Fabrizio, "A new definition of fractional derivative without singular kernel," *Progress in Fractional Differentiation & Applications*, vol. 1, no. 2, pp. 73–85, 2015.
[27] A. Atangana and D. Baleanu, "New fractional derivatives with nonlocal and non-singular kernel: theory and application to heat transfer model," *arXiv preprint arXiv:1602.03408*, 2016.
[28] I. Ameen, D. Baleanu, and H. M. Ali, "An efficient algorithm for solving the fractional optimal control of sirv epidemic model with a combination of vaccination and treatment," *Chaos, Solitons & Fractals*, vol. 137, p. 109892, 2020. DOI:10.1016/j.chaos.2020.109892
[29] M. A. Krasnosel'skii, "Two remarks on the method of successive approximations," *Uspekhi matematicheskikh nauk*, vol. 10, no. 1, pp. 123–127, 1955.
[30] A. Atangana and S. Qureshi, "Modeling attractors of chaotic dynamical systems with fractal–fractional operators," *Chaos, solitons & fractals*, vol. 123, pp. 320–337, 2019. DOI:10.1016/j.chaos.2019.04.020
[31] B. Ghosh, "Fractional order modeling of ecological and epidemiological systems: ambiguities and challenges," *The Journal of Analysis*, vol. 33, pp. 341–366, 2025. DOI:10.1007/s41478-024-00836-y
[32] D. Roy and B. Ghosh, "Dimensionally homogeneous fractional order rosenzweig–macarthur model: a new perspective of paradox of enrichment and harvesting," *Nonlinear Dynamics*, vol. 112, no. 20, pp. 18137–18161, 2024. DOI:10.1007/s11071-024-09959-0
[33] M. Nagumo, "Über die lage der integralkurven gewöhnlicher differentialgleichungen," *Proceedings of the Physico-Mathematical Society of Japan. 3rd Series*, vol. 24, pp. 551–559, 1942.
[34] S. Ulam, *Problems in modern mathematics*. New York: Dover Publications, Inc., 2004.
[35] A. Kilbas, H. Srivastava, and J. Trujillo, *Theory and applications of fractional differential equations*. New York: Elsevier, 2006.
[36] W. H. Fleming and R. W. Rishel, *Deterministic and stochastic optimal control*. New York: Springer, 2012. DOI:10.1007/978-1-4612-6380-7
[37] H. Schättler and U. Ledzewicz, *Optimal control for mathematical models of cancer therapies*. New York: Springer, 2015. DOI:10.1007/978-1-4939-2972-6
[38] I. L. Correa-Escudero *et al.*, "Correcting dimensional mismatch in fractional models with power, exponential and proportional kernel: Application to electrical systems," *Results in Physics*, vol. 40, p. 105867, 2022. DOI:10.1016/j.rinp.2022.105867

Appendix

The incorporation of the memory rate parameter with inverse time dimensions is essential in any epidemiological model involving time-fractional derivatives, including those using non-singular kernels such as the exponential kernel in the Caputo–Fabrizio derivative or the Mittag–Leffler kernel in the Atangana–Baleanu derivative in the Caputo sense [38]. This inclusion is critical to ensuring dimensional balance and consistency within the model.

A dimensional imbalance arises when classical integer-order time derivatives (d/dt), which have dimensions of inverse time (e.g., $(1/T)$), are directly replaced by fractional derivatives of order $\alpha \in (0,1)$ that scale differently, typically with dimension $(1/T)^\alpha$. This introduces a mismatch in model units, leading to dimensional inconsistency, mathematically invalid equations, distortion in the physical interpretation of model parameters, and a loss of biological relevance in model predictions.

For instance, the Caputo–Fabrizio fractional derivative of order α has the effective dimension:

$$[\,{}^{CF}D_t^\alpha f(t)\,] \sim \frac{[f(t)]}{T^\alpha}, \quad \text{for } 0 < \alpha < 1.$$

Proof. The Laplace transform of the Caputo–Fabrizio derivative is given by:

$$\mathcal{L}\left\{{}^{CF}D_t^\alpha f(t)\right\}(s) = M(\alpha)\frac{s}{s+\lambda}\tilde{f}(s),$$

where $M(\alpha)$ is a normalization constant with $M(0) = M(1) = 1$, and $\lambda = \frac{\alpha}{1-\alpha}$. Here, $s \sim 1/T$, $\tilde{f}(s) \sim [f]\cdot T$, and $\frac{s}{s+\lambda} \sim (1/T)^\alpha$ behavior can be inferred for small α. □

Alternative Proof. The Caputo–Fabrizio exponential kernel for fractional parameter $\alpha \in (0,1)$ is:

$$e^{-\frac{\alpha t}{1-\alpha}} = \frac{1}{(e^t)^{\frac{\alpha}{1-\alpha}}} \approx \frac{1}{(1+t+\frac{t^2}{2!}+\frac{t^3}{3!}+\cdots)^\alpha} \leq \frac{1}{(1+t)^\alpha} \leq \frac{1}{t^\alpha}.$$

Since $t \sim T$, this implies the effective dimension of the Caputo–Fabrizio derivative is:

$$[\,{}^{CF}D_t^\alpha f(t)\,] \sim \frac{[f(t)]}{T^\alpha}, \quad \text{for } 0 < \alpha < 1.$$

This supports the conclusion that the Caputo–Fabrizio derivative modifies the time scaling to effectively behave like a derivative of order α.

Similarly, the Atangana–Baleanu fractional derivative in the Caputo sense has the typical dimension:

$$[\,{}^{ABC}D_t^\alpha f(t)\,] \sim \frac{[f(t)]}{T^\alpha}, \quad \text{for } 0 < \alpha < 1.$$

□

Proof. Using a scaling argument, let $f(t) = t^\gamma$, which implies $[f(t)] = T^\gamma$. The Atangana–Baleanu–Caputo time-fractional derivative for a power-law function is:

$${}^{ABC}D_t^\alpha t^\gamma = \frac{B(\alpha)\Gamma(\gamma+1)}{(1-\alpha)\Gamma(\gamma+1-\alpha)}t^{\gamma-\alpha}.$$

This implies:

$${}^{ABC}D_t^\alpha t^\gamma \propto t^{\gamma-\alpha}.$$

Thus, the dimension becomes:

$$[\,{}^{ABC}D_t^\alpha t^\gamma\,] = T^{\gamma-\alpha} = \frac{[f(t)]}{T^\alpha}.$$

Hence, the Atangana–Baleanu derivative reduces the time exponent by α, and its effective dimension is:

$$[\,{}^{ABC}D_t^\alpha f(t)\,] \sim \frac{[f(t)]}{T^\alpha}, \quad \text{for } 0 < \alpha < 1.$$

Therefore, directly replacing the classical time derivative ($d/dt \sim 1/T$) with a time-fractional derivative—such as the Caputo–Fabrizio or Atangana–Baleanu in the Caputo sense—without incorporating a memory rate parameter leads to dimensional inconsistency. This compromises the mathematical integrity of the model and diminishes its relevance and applicability to real-world biological or epidemiological systems.

Thus, the inclusion of an appropriately scaled memory rate parameter is not only mathematically sound and technically justified, but also critically important for ensuring dimensional balance and consistency within the model framework. □